Paralemmin, a Prenyl-Palmitoyl–anchored Phosphoprotein Abundant in Neurons and Implicated in Plasma Membrane Dynamics and Cell Process Formation

Christian Kutzleb,* Gabriele Sanders,* Raina Yamamoto,* Xiaolu Wang,* Beate Lichte,* Elisabeth Petrasch-Parwez,‡ and Manfred W. Kilimann*

*Institut für Physiologische Chemie, and ‡Institut für Anatomie, Ruhr-Universität Bochum, D-44780 Bochum, Germany

Abstract. We report the identification and initial characterization of paralemmin, a putative new morphoregulatory protein associated with the plasma membrane. Paralemmin is highly expressed in the brain but also less abundantly in many other tissues and cell types. cDNAs from chicken, human, and mouse predict acidic proteins of 42 kD that display a pattern of sequence cassettes with high inter-species conservation separated by poorly conserved linker sequences. Prenylation and palmitoylation of a COOH-terminal cluster of three cysteine residues confers hydrophobicity and membrane association to paralemmin. Paralemmin is also phosphorylated, and its mRNA is differentially spliced in a tissue-specific and developmentally regulated manner. Differential splicing, lipidation, and phosphorylation contribute to electrophoretic heterogeneity that results in an array of multiple bands on Western blots, most notably in brain. Paralemmin is associated with the cytoplasmic face of the plasma membranes of postsynaptic specializations, axonal and dendritic processes and perikarya, and also appears to be associated with an intracellular vesicle pool. It does not line the neuronal plasmalemma continuously but in clusters and patches. Its molecular and morphological properties are reminiscent of GAP-43, CAP-23, and MARCKS, proteins implicated in plasma membrane dynamics. Overexpression in several cell lines shows that paralemmin concentrates at sites of plasma membrane activity such as filopodia and microspikes, and induces cell expansion and process formation. The lipidation motif is essential for this morphogenic activity. We propose a function for paralemmin in the control of cell shape, e.g., through an involvement in membrane flow or in membrane–cytoskeleton interaction.

Key words: farnesylation • lipidation • cortical cytoskeleton • membrane traffic • synapse

Neurons possess an elaborate plasma membrane architecture. The enormous arborization of these cells not only implies a very high ratio of cell surface to volume in a highly defined morphology, but this surface is also—particularly at pre- and postsynaptic contacts—subdivided into a complex mosaic of subdomains with differential compositions of membrane proteins. Moreover, synapses are hotspots of fast and strictly regulated membrane dynamics. To construct, maintain, and reshape the complex plasma membrane architecture of neurons, an interplay between the plasma membrane, exo/endocytotic vesicles, and the cortical cytoskeleton must permit or mediate membrane flow at dynamic sites but stabilize the static regions. Demands on the control of plasma membrane shape and composition are particularly challenging at synapses, where rapid membrane flows occur within the constraints of a subtle micromorphology.

To identify new protein components of synapses, we have previously raised antisera against synaptic plasma membranes obtained by subcellular fractionation and screened brain cDNA expression libraries for clones whose expression products reacted immunopositive with these sera. Among the proteins newly identified in this immunoscreen were: amphiphysin (Lichte et al., 1992), for which an involvement in neurotransmitter vesicle re-endocytosis has recently emerged (Shupliakov et al., 1997), and that has also been identified as an autoantigen in paraneoplastic neurological autoimmune diseases (De Camilli et al., 1993; Dropcho, 1996); myosin V, an unconventional myosin (Sanders et al., 1992) that is affected by genetic defects of exocytosis in yeast, mice, and humans (Johnston et al., 1991; Mercer et al., 1991; Pastural et al., 1997), and

Address all correspondence to Manfred W. Kilimann, Institut für Physiologische Chemie, Ruhr-Universität Bochum, D-44780 Bochum, Germany. Tel.: 49-234-700-7927. Fax: 49-234-7094-193. E-mail: manfred.kilimann@ruhr-uni-bochum.de

functions as a motor protein in intracellular membrane vesicle transport (e.g., in the extension of filopodia [Wang et al., 1996] and at synapses [Prekeris and Terrian, 1997]); and a homologue of μ-adaptins that presumably is a subunit of a new type of vesicle coat involved in intracellular membrane traffic (Wang and Kilimann, 1997). About 50% of the clones picked up in this immunoscreen encoded known proteins: GAP-43; MARCKS; N-CAM; the prion protein as established proteins associated with neuronal plasma membranes; CAP-23, a cortical cytoskeleton-associated protein related to GAP-43; the molecular chaperones hsp70 and cyclophilin; the cytoskeletal proteins MAP-1B, MAP-2, and ankyrin-B; and calmodulin. The only obviously unspecific protein was a ferredoxin of presumably mitochondrial origin. Notably, a significant fraction of the novel and known proteins found in our immunoscreen are implicated in membrane traffic or membrane–cytoskeleton interaction.

In the present article, we describe the identification of another new protein associated with synaptic plasma membranes, paralemmin, and its initial molecular, morphological and functional characterization. Paralemmin is a hydrophilic protein anchored to membranes through a COOH-terminal CaaX lipidation motif. It is highly expressed in neurons; it is found at the plasma membranes of postsynaptic specializations, axonal and dendritic processes, and perikarya. Paralemmin is also detectable at lower levels in many other tissues and cell types. Several of its molecular and morphological properties are reminiscent of GAP-43 and MARCKS, proteins implicated in plasma membrane dynamics. Overexpression of paralemmin in several cell lines induces cell expansion and process formation, and we therefore propose a function for paralemmin, e.g., as a SNAP receptor (SNARE)[1] or as a membrane anchor for the cortical cytoskeleton, in the control of cell shape.

Materials and Methods

cDNA Cloning, Sequencing, and RNA Analysis

Rabbit antisera against synaptic plasma membrane preparations from chicken brain (age, 7–10 d) were raised and used for immunoscreening of chicken brain cDNA expression libraries in λgt11 as described (Lichte et al., 1992). Conventional procedures were used for hybridization rescreening of chicken, human (human fetal brain; Stratagene, La Jolla, CA), and mouse brain (Hoesche et al., 1993) cDNA libraries and for DNA sequencing. Purification of RNA from various chicken and mouse tissues and cell lines, oligo (dT) cellulose chromatography, Northern blotting, and blot hybridization at high stringency were also performed according to standard procedures (Hoesche et al., 1993, 1995). Human multiple tissue Northern blots were purchased from CLONTECH Laboratories, Inc. (Palo Alto, CA) and hybridized at high stringency according to the manufacturer's instructions. For reverse-transcribed polymerase chain reaction (RT-PCR), total RNA or poly(A)+ RNA from mouse, human, or chicken tissues were reverse transcribed and amplified, and the PCR products sequenced as described (Wüllrich et al., 1993; Burwinkel et al., 1996).

Mouse cell lines NS20Y, N1E115, NH15CH2, 108CC15, and L929 were cultivated in DME supplemented with 10% FCS at 8% CO_2. To induce morphological differentiation of neuroblastoma cells, the serum concentration was reduced to 0.5% or 0.25%, and culture continued for 7 d. To stimulate protein kinase–mediated signal pathways, 10 μM forskolin/0.5 μM IBMX (3-isobutyl-1-methylxanthine), 0.6 μM of the calcium ionophore A23187, or a concentration series of 0.1 nM to 1 μM of the phorbol ester 12-O-tetradecanoylphorbol-13-acetate (TPA), respectively, were added and culture continued for 24 h. Northern blot analysis demonstrated slight decreases in mRNA abundance under either condition, in parallel to similar decreases of synapsin I mRNA abundance (Hoesche et al., 1995) and therefore presumably unspecific in nature. The same Northern blots used by Hoesche et al. (1995) were used for paralemmin mRNA hybridization, allowing a direct comparison with synapsin I mRNA abundance as control.

Monospecific Antisera and Immunoblotting

A rabbit antiserum against chicken paralemmin (amino acid 16 to COOH terminus without exon 8) was raised against the β-galactosidase fusion protein of the initial cDNA clone ch10.12.1 as described (Lichte et al., 1992). Two rabbit sera (Nos. 2 and 10) and a chicken serum (HB) were raised against a partial mouse paralemmin sequence (amino acids 15–242 without exon 8) obtained by RT-PCR and fused to glutathione-S-transferase (GST) in the bacterial expression vector pGEX-3X (Pharmacia Biotech, Inc., Piscataway, NJ). Two rabbit sera were raised against a synthetic peptide (mouse paralemmin amino acids 13–27, ERLQAIAEKRRKQAE, plus a COOH-terminal cysteine) coupled to keyhole limpet hemocyanin either with glutaraldehyde (serum No. 8) or with 3-maleimidoacetic acid *N*-hydroxysuccinimide ester (MBS; No. 12). A rabbit serum against recombinant chicken amphiphysin has been described (Lichte et al., 1992). An mAb against the synaptic vesicle protein SV2 (mouse IgG1, hybridoma SP2/0; Feany et al., 1992) was the gift of Dr. K.M. Buckley (Harvard Medical School, Boston, MA).

For affinity purification of anti–mouse paralemmin sera, the GST fusion protein was proteolytically cleaved with coagulation factor X (Boehringer Mannheim Corp., Indianapolis, IN), the GST moiety removed by chromatography over glutathione Sepharose, and the paralemmin moiety coupled to tresyl Sepharose (both resins from Sigma Chemical Co., St. Louis, MO). Sera (100 μl) were passed over the paralemmin column (1.4 ml), and bound antibodies eluted sequentially with 0.2 M glycine/HCl, pH 2.8, and 2 M $MgCl_2$. Antibody-containing fractions were pooled, dialyzed against PBS, and then stored at −70°C. Mock affinity-purified preimmune sera for controls were prepared in the same way. The specificity of affinity-purified antibodies was confirmed by blocking experiments. Preincubation with recombinant paralemmin completely abolished the reactivity of the antibodies in immunoblot, immunofluorescence, and immunocytochemistry experiments.

SDS-PAGE and immunoblotting onto nitrocellulose were performed by standard methods, and immunoblots developed with alkaline phosphatase–coupled secondary antibodies (Dianova, Hamburg, Germany) and the 5-bromo-4-chloro-3-indolyl-phosphate/*para*-nitrotetrazolium-blue color reaction.

Subcellular Fractionation, Deglycosylation, Triton X-114 Phase Partitioning, and Hydroxylamine Hydrolysis

Tissue homogenates for immunoblotting were prepared by homogenization in 0.32 M sucrose, 1 mM EDTA, 10 mM Tris, pH 7.4, 0.5 mM PMSF, 2 μg/ml pepstatin A, 2 μg/ml leupeptin, using a glass-Teflon homogenizer or, for muscle and heart, a turning knife homogenizer. To prepare extracts from cell lines NS20Y, L929, and PC12, cells were rinsed with PBS, scraped from the dish in 20 mM Tris, pH 7.4, 2 mM EDTA, 0.5 mM PMSF, 2 μg/ml pepstatin A, 2 μg/ml leupeptin, and sheared by 10 passages through a G27 syringe. These homogenates were spun for 3 min at 3,000 rpm (900 *g*) in a microcentrifuge, and the supernatant stored at −70°C.

Membrane and cytosolic fractions were prepared from cell line extracts (900 *g* supernatants) by a 120,000 *g* centrifugation for 30 min at 4°C (Chapman et al., 1992). After resuspending in homogenization buffer and measuring the protein concentration, the fractions were diluted in SDS-PAGE sample buffer and equal protein quantities run on a 9% polyacrylamide gel.

Subcellular fractionation leading to the purification of synaptic plasma membranes was carried out by the method of Babitch et al. (1976), and synaptic vesicles were purified according to Hell et al. (1988). Deglycosylation reactions were performed on chicken synaptic plasma membrane fractions 0.4/0.6 or 0.6/0.8 and on fetuin (Sigma Chemical Co.) as positive

1. *Abbreviations used in this paper*: GFP, green fluorescent protein; GST, glutathione-S-transferase; nt, nucleotide(s); RT-PCR, reverse-transcribed polymerase chain reaction; SNARE, SNAP receptor.

control, with *N*-glycosidase F (*Flavobacterium meningosepticum*), O-glycosidase (*Diplococcus pneumoniae*), and neuraminidase (*Vibrio cholerae*), all from Boehringer Mannheim Corp., under the conditions suggested by the manufacturer.

Triton X-114 phase partitioning was carried out according to Bordier (1981) and Pryde (1986). For hydroxylamine hydrolysis, synaptic plasma membranes (50–130 μg protein) were incubated in 1 M hydroxylamine, pH 7.5, 1% SDS, at 37°C for 1.5–4 h. A control incubation was carried out in parallel in 1 M Tris, pH 7.5, 1% SDS. After incubation, the samples were adjusted to final concentrations of 1% Triton X-114, 150 mM NaCl, 1 mM $CaCl_2$, 10 mM Tris, pH 7.5, by addition of concentrated stock solutions, and then subjected to phase partitioning. Before SDS-PAGE, detergents were removed from the fractions by TCA precipitation, washing of the protein precipitates with ice-cold acetone, and then resuspension in sample buffer. The entire fractions were then run on a 9% polyacrylamide gel and analyzed by Western blotting. Phase partitioning was either carried out on virtually undiluted samples (end concentrations of 700 mM hydroxylamine or Tris, respectively) or after dilution to end concentrations of 50 mM hydroxylamine or Tris, to test for possible effects of high hydroxylamine concentrations on phase partitioning. Under both conditions, the hydroxylamine effect was the same (transition of half of paralemmin into the aqueous phase), whereas paralemmin was nearly completely retained in the detergent phase if Triton X-114 partitioning in 50 mM hydroxylamine was performed immediately after hydroxylamine addition.

Expression and Metabolic Labeling of Recombinant Chicken Paralemmin in COS-7 Cells

Chicken cDNA clone 10.12.1-dT1, extending from nucleotide (nt) 1 to 1,362, and encompassing the entire coding sequence without exon 8, was excised from λgt11 by EcoRI, blunted with Klenow enzyme, and then inserted into the SmaI site of eukaryotic expression vector pSVL (Pharmacia Biotech Corp.). Recombinant plasmid was transfected into COS-7 cells by the DEAE–dextran/DMSO method. After the DMSO shock and medium exchange, cells were cultivated in 6-well plates in medium A (DME with 10% FCS, 250 μg/ml streptomycin, 250 units/ml penicillin) for 48 h before the addition of metabolic label. Labeling with [^{3}H]mevalonolactone (DuPont-NEN, Boston, MA) according to Adamson et al. (1992) was performed in medium C (medium A supplemented with 50 μM mevinolin [lovastatin; gift of Dr. Alberts, Merck & Co., Inc., Rahway, NJ], an inhibitor of HMG-CoA reductase). Cells were preincubated with medium C for 3 h, and then labeled with 0.1 mCi [^{3}H]mevalonolactone in 1 ml medium C per well overnight. Labeling with [^{3}H]palmitate (DuPont-NEN) was carried out according to Karnik et al. (1993) at a reduced FCS concentration to lower the background of unlabeled palmitate. For this purpose, cells were preincubated for 5 h in medium A without FCS and 30 min in medium A with 1% FCS, and then grown in 0.75 ml medium A with 1% FCS plus 0.45 mCi [^{3}H]palmitate per well. For labeling with [^{35}S]methionine and [^{35}S]cysteine, cells were grown overnight in 0.75 ml of medium A (without cold methionine and cysteine) plus 0.75 mCi Tran^{35}S-Label (ICN Biomedicals, Costa Mesa, CA) per well. Cells were harvested by washing twice with 1 ml PBS and lysing with 0.5 ml 1% Triton X-100/0.5% deoxycholate/100 mM NaCl/20 mM Tris (pH 7.4)/ 3 mM $MgCl_2$/3 mM PMSF for 30 min on ice. The lysate was spun for 10 min at 12,000 rpm in a microliter centrifuge to remove debris before storage at −70°C, immunoprecipitation, and then analysis by SDS-PAGE. Electrophoresis gels were soaked in Amplify (Amersham Corp., Arlington Heights, IL) before drying and exposure to X-ray film.

Metabolic Labeling of Paralemmin with ^{32}P

NS20Y cells (10^6 per dish) were seeded in 35-mm petri dishes and cultivated for 48 h. After replacement of the culture medium by 500 μl of labeling buffer (phosphate- and serum-free DME, supplemented with 10 μM sodium phosphate, 0.5% BSA, and 200 μCi [^{32}P]phosphoric acid [ICN Biomedicals] per dish), the cultivation was continued for another 4 h. Cells were washed twice with 2 ml Locke buffer (140 mM NaCl, 2 mM $MgCl_2$, 2 mM $CaCl_2$, 5.6 mM KCl, 5.6 mM glucose, 15 mM Hepes, pH 7.4), lysed in 500 μl RIPA buffer (1% Triton X-100, 0.5% sodium deoxycholate, 150 mM NaCl, 3 mM $MgCl_2$, 5 mM EGTA, 20 mM Tris-HCl, pH 7.4, supplemented with 0.5 mM PMSF, 2 μg/ml leupeptin, 2 μg/ml pepstatin A, 1 mM sodium vanadate, 50 mM NaF, 10 mM *para*-nitrophenylphosphate) on ice for 30 min, and the soluble extract obtained by centrifugation at 14,000 *g* for 30 min at 4°C.

For immunoprecipitation, the extract was pre-cleared by incubation, for 1 h each, with 1 μl crude preimmune serum and 25 μl pansorbin (Calbiochem-Novabiochem Corp., La Jolla, CA). After pelleting the pansorbin, the supernatant was incubated with 1 μl of antiserum overnight followed by 30 μl pansorbin for 2 h. All incubations were at 4°C on an end-over-end mixer. The pansorbin pellet was washed three times in RIPA buffer, resuspended in SDS sample buffer and subjected to SDS-PAGE (9% polyacrylamide). After semidry blotting onto nitrocellulose sheets, phosphoproteins were detected by autoradiography of the blots with intensifying screens at −70°C for ~3 d. The blots were subsequently developed for immunodetection of paralemmin.

Immunofluorescence Microscopy in Cell Culture

Cell lines were grown at 37°C in DME supplemented with 10% FCS and 50 μg/ml streptomycin, 50 IU/ml penicillin, 2 mM L-glutamine, 1 mM pyruvate, in a water-saturated atmosphere with 8% CO_2. For PC12 cells, serum concentrations were 5% FCS and 10% horse serum. Cell were used 2 d after plating. To induce morphological differentiation of NS20Y cells, medium with 10% FCS was replaced after 2 d by medium with 0.25% FCS, and culture continued for another 7 d. Cells were seeded on glass coverslips coated with rat-tail collagen (Sigma Chemical Co.) in 24-well plates. The FCS-containing medium was removed by rinsing the cells twice in Locke buffer, followed by fixation in 4% PFA in PBS at room temperature. Cells were permeabilized with methanol at −20°C for 6 min. Before incubation with primary antibodies (diluted in PBS with 1% BSA), a preincubation for 10 min with 10% normal goat serum in PBS was carried out to reduce background. Anti-paralemmin was visualized with a biotinylated goat anti–rabbit secondary antibody (Vector Labs, Inc., Burlingame, CA) followed by streptavidin-FITC. In double-immunofluorescence experiments, GAP-43 (mAb 91E12 from Boehringer Mannheim Corp.) was visualized with a Texas red–conjugated goat anti–mouse antibody (Dianova). All incubations were for 1–2 h with extensive washings in between. Coverslips were finally mounted in Mowiol (Calbiochem-Novabiochem Corp.) supplemented with 50 mg/ml diazo-bicyclooctane (Merck, Darmstadt, Germany) and 25 mg/ml propylgallate to reduce bleaching of the fluorescent dye. Specimens were viewed on an Axiophot I microscope (Carl Zeiss, Inc., Thornwood, NY).

Functional Expression Experiments

Full-length (amino acids 2–383) and COOH-terminally truncated (amino acids 2–368) paralemmin sequences, both including exon 8, were amplified from mouse brain RNA by RT-PCR. The paralemmin sequences were fused with the NH_2-terminal sequence MEQKLISEEDLGSKL that includes the myc epitope tag, and the whole construct inserted between the HindIII and XbaI sites of pcDNA3.1/Zeo+ (Invitrogen Corp., Carlsbad, CA; myc tag engineering by G. Dodt, Institut für Physiologishe Chemie, University of Bochum, Bochum, Germany). Recombinant plasmid clones were verified by sequencing of the complete inserts. L929, COS-7, PC12, and GM5756t (Dodt et al., 1995) cells were transfected by the DEAE–dextran method. Cells were incubated with the DEAE–dextran–DNA complex for 4 h, grown for ≤3 d, and then processed for immunofluorescence microscopy as described above. The myc immuno-tag was visualized with the 9E10 mAb (Evan et al., 1985; gift of G. Dodt), and F-actin with a TRITC-phalloidin conjugate (Sigma Chemical Co.). In experiments using TRITC-phalloidin, cells were permeabilized with 0.2% Triton X-100 in PBS for 1 min at room temperature. Control transfections used the green fluorescent protein (GFP) expression plasmid pEGFP-C1 (CLONTECH Labs.).

Immunocytochemistry

Rats were perfused transcardially with 2.5% glutaraldehyde, 1.5% formalin, 0.1 M sodium phosphate, pH 7.4, for 30 min at 38°C. Fixation was followed by a 10-min perfusion with 0.15 M sucrose, 0.1 M sodium phosphate, pH 7.4. The tissue was removed, submerged in the latter solution and cut into 2-mm slices. For immunocytochemical staining, 50-μm vibratome sections from these slices were incubated in free-floating fashion for 30 min in PBS with 10% normal goat serum and 0.3% Triton X-100, followed by incubation for 48 h with primary antibody in the same solution, all at 4°C. After repeated rinsing with PBS and blocking with 0.1% BSA in PBS for 60 min, sections were incubated for 24 h with biotinylated goat anti–rabbit secondary antibody. After washing and blocking, the sections were finally incubated for 4 h with the avidin-biotinylated peroxidase complex (ABC; Vector Labs, Inc.). Peroxidase activity was visual-

ized with 3,3′-diaminobenzidine followed by an enhancement with 0.1% osmium tetroxide.

For light microscopy, sections were drawn on subbed slides, quickly dehydrated and coverslipped. For electron microscopy, the same solutions were used with the omission of Triton X-100 and the sections were flat embedded in araldite after the immunocytochemical procedure. Series of alternating semithin and ultrathin sections were taken from the embedded tissues. Every second semithin section was counterstained with 1% toluidine blue. Ultrathin sections were contrasted with uranyl acetate and lead citrate.

Extensive controls were performed to verify the specificity of immunocytochemical staining. The same characteristic ultrastructural localization of paralemmin-immunoreactive material in brain was seen if perfusion was carried out with 4% PFA, 0.05% glutaraldehyde, 0.2% picric acid in 0.1 M sodium phosphate, pH 7.4, at room temperature, or if sections were incubated during the staining procedure in the presence of 1% Triton X-100. Under both conditions, however, structural conservation was poorer so that the procedure described above was preferred. The same staining patterns were obtained with two different affinity-purified rabbit sera and also with the corresponding whole sera. No staining was obtained when sections were incubated with preimmune sera or when immune sera were pre-incubated with recombinant paralemmin. In contrast, pre-incubation of paralemmin antibodies with the recombinant new protein, HSB, that is partially homologous to paralemmin and mentioned in the first Results chapter, did not abolish immunodetection of paralemmin, neither on Western blots (see Fig. 5 *B*) nor in immunocytochemistry of tissue sections. This demonstrated that cross-reactivity with this related antigen does not contribute to the anti-paralemmin staining described here.

Results

cDNA Cloning and Predicted Primary Structure of Paralemmin from Chicken, Human, and Mouse

Chicken brain cDNA expression libraries were immunoscreened with an antiserum raised against the detergent phase of synaptic plasma membranes subjected to Triton X-114 phase partitioning. The detergent phase contains the hydrophobic proteins of this membrane preparation, in particular intrinsic membrane proteins. One of the cDNA clones whose expression product reacted immunopositive with this serum was designated ch10.12.1, and it was selected for further characterization because Northern blot hybridization indicated that the corresponding mRNA is most abundantly expressed in brain (see below). By several rounds of hybridization rescreening, cDNAs were isolated that yield the complete coding sequences of chicken, human, and mouse paralemmin (Figs. 1 and 2).

The cDNAs predict highly charged proteins with an excess of acidic residues, particularly glutamate (pI values, 4.7–4.9), but few cysteines and aromatic amino acids. There is only one conserved residue each of tyrosine, phenylalanine, and tryptophan in the constitutively expressed sequences, and two additional conserved tyrosines occur in the differentially spliced region (see below). Amino acid sequence identity is 54% between chicken and human, 52% between chicken and mouse, and 80% between human and mouse. Sequence alignment reveals several regions of very high conservation even between mammals and birds that are separated, apparently, by poorly conserved linker sequences (Fig. 2 *A*). The proteins from the three species are of very similar size (383–387 amino acids) in spite of a considerable divergence of sequences and also lengths in individual linker regions.

Most of the paralemmin sequence is predicted to have high α helix potential. The highly conserved NH_2-terminal 105 amino acids display a striking periodicity of acidic, basic, hydrophobic, and glutamine residues, with two potential leucine zippers, and are predicted to have a high coiled-coil potential with scores between 1.3 and 2.15 (Fig. 2 *B*). Database searches confirmed a loose sequence similarity of this region with the coiled-coil regions of various myosin heavy chains, tropomyosin, and the intermediate

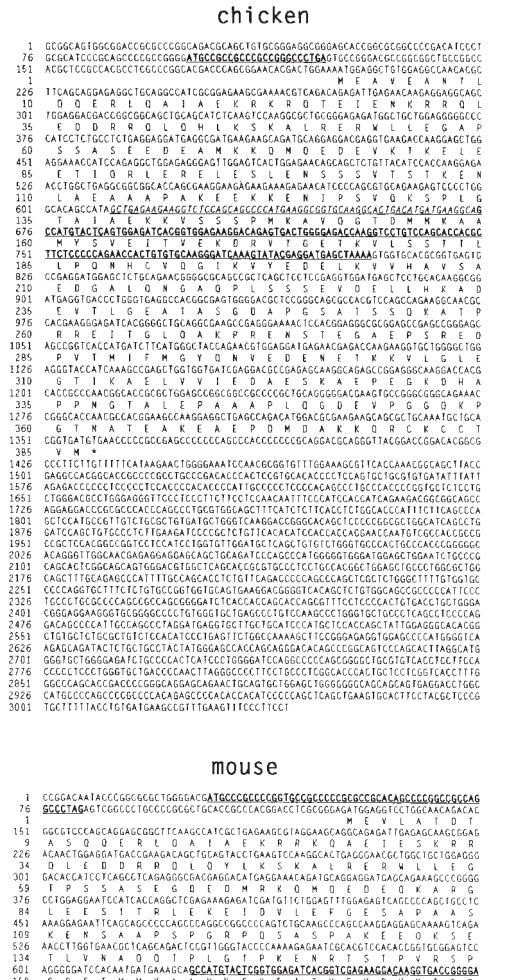

Figure 1. cDNA and deduced amino acid sequences of chicken and mouse paralemmin. Short reading frames in the 5′ untranslated regions and the differentially spliced sequences corresponding to human exon 8 are underlined and printed in bold. The differentially spliced chicken exon 7 sequence is underlined and italicized. The human cDNA sequence has been incorporated into the gene sequence published elsewhere (Burwinkel et al., 1998). These sequence data are available from GenBank/EMBL/DDBJ under accession Nos. Y14769–Y14771.

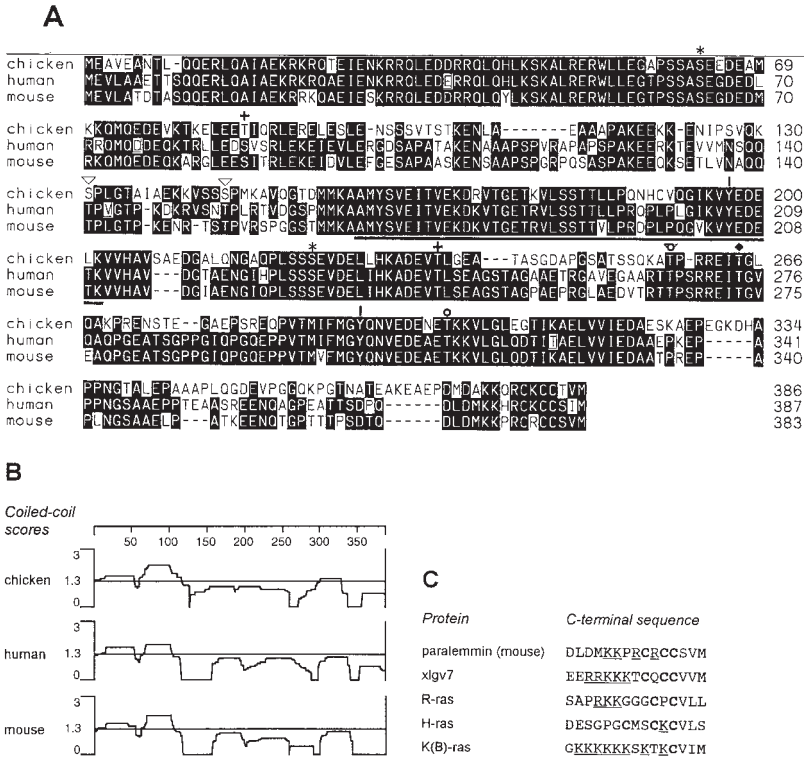

Figure 2. (*A*) Alignment of the predicted amino acid sequences of chicken, human, and mouse paralemmin. The sequence subject to differential splicing of exon 8 is underlined. Candidate phosphorylation sites conserved in all three species that fit consensus sequences for protein kinase substrates are marked by the following symbols: +, casein kinase I; *, casein kinase II; ◆, protein kinase A and CaM kinase II; ○, protein kinase C; △, proline-directed kinases; |, tyrosine kinases. (References for consensus sequences: Kennelly and Krebs, 1991; Songyang et al., 1995, 1996.) (*B*) Coiled-coil potential of chicken, human, and mouse paralemmin determined with the DNASTAR Protean software (Macintosh v. 3.04). (*C*) Alignment of the COOH-terminal amino acid sequences of paralemmin, xlgv7, and three Ras isoforms illustrating sequence motifs involved in membrane anchoring. Cysteine residues are in bold print and basic residues are underlined. Sequences are taken from Kloc et al. (1991) and references therein.

filament–associated proteins trichohyalin and involucrin. More pronounced sequence similarity with this and additional, but not all regions of the paralemmin sequence is displayed by another novel protein, HSB, that is currently under study in our laboratory. No other related sequences, e.g., from yeast, were found in the database. A partial sequence (human paralemmin amino acids 203–214; IKVYEDETKVVH) is reminiscent of a sequence stretch (MKVQQELDETKIVLH) in a lipid-anchored SNARE protein, Ykt6p, that is involved in ER–Golgi transport (McNew et al., 1997). The COOH terminus of paralemmin carries a characteristic CaaX prenylation consensus sequence (Fig. 2 *C*) that will be addressed in more detail below.

In all three species, the coding sequences are preceded by GC-rich 5′ untranslated regions. The chicken and mouse 5′ untranslated sequences contain short reading frames (7 and 17 triplets, respectively; Fig. 1). In the mouse, this short reading frame is in register with the coding sequence and thus closes the 5′ end of the long reading frame. Short reading frames in 5′ untranslated mRNA sequences have been implicated in the control of translation efficiency.

Paralemmin mRNA Expression: Tissue Specificity, Differential Splicing, and Developmental Regulation

Northern blot analysis of chicken, human and mouse RNAs (Fig. 3) demonstrates an mRNA of ~3,200 nt in all three species. With chicken RNAs, the hybridization signal is prominent in forebrain and cerebellum, less intense in adrenal gland and heart, and weak or undetectable in the other tissues analyzed. On the human Northern blots, the paralemmin mRNA is detectable in all tissues analyzed, again with the highest expression in brain (besides testis) and intermediate abundance in heart and adrenal gland. Kidney is the only tissue analyzed in which a second mRNA band of ~2,500 nt can be seen.

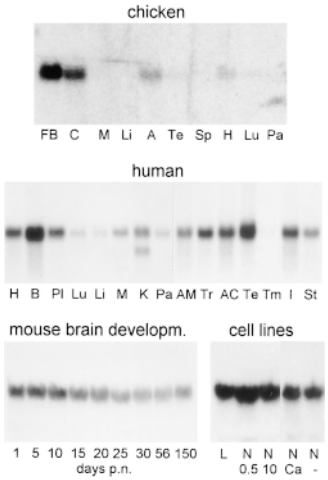

Figure 3. Northern blot analysis of paralemmin mRNA expression. Blots carry 10 μg poly(A)+ RNA from chicken tissues, 2 μg poly(A)+ RNA from human tissues, 20 μg total RNA from mouse brain, and 50 μg total RNA from cell lines, respectively. Tissues of origin are forebrain (*FB*), cerebellum (*C*), skeletal muscle (*M*), liver (*Li*), whole adrenal gland (*A*), testis (*Te*), spleen (*Sp*), heart (*H*), lung (*Lu*), pancreas (*Pa*), whole brain (*B*), placenta (*Pl*), kidney (*K*), adrenal medulla (*AM*), thyroid gland (*Tr*), adrenal cortex (*AC*), thymus (*Tm*), small intestine (*I*), and stomach (*St*). RNA from developing mouse brain was isolated on the days of postnatal age indicated. Cell lines are: (*L*) L929 mouse fibroblast cells; (*N 0.5*) NS20Y mouse neuroblastoma cells grown for 7 d at low serum (0.5%); (*N 10*) NS20Y cells grown for 7 d at high serum (10%); (*N Ca*) NS20Y cells treated with calcium ionophore A23187 for 24 h; (*N −*) NS20Y cells grown without A23187 for 24 h.

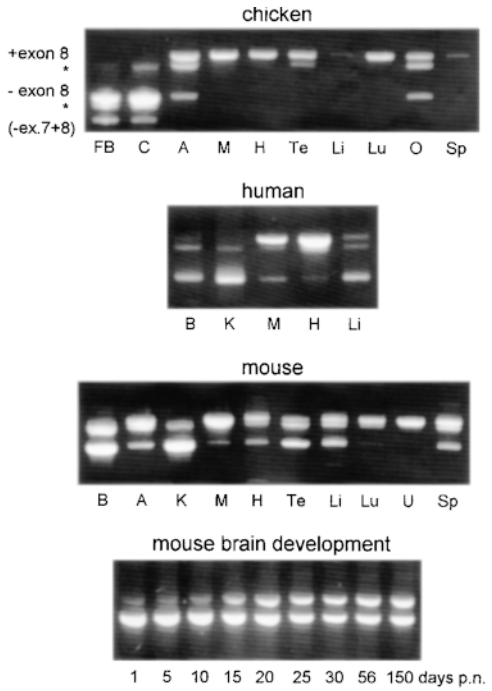

Figure 4. Differential splicing of paralemmin mRNA analyzed by RT-PCR. The differentially spliced region of chicken, human, and mouse paralemmin mRNA was amplified by RT-PCR, and amplification products resolved by agarose gel electrophoresis and stained with ethidium bromide. The first and third bands from the top represent RNAs with and without exon 8, and the second band from the top (*asterisk*) is a heteroduplex of both. Chicken forebrain and cerebellum additionally yield a product lacking both exons 7 and 8, and its heteroduplex (*asterisk*) with the "minus exon 8" PCR product. Tissues are designated as in Fig. 3, additional tissues are ovary (*O*) and uterus (*U*).

The developmental course of paralemmin mRNA expression in postnatal mouse brain is shown at the bottom of Fig. 3. mRNA abundance is highest in neonatal brain and declines to ~50% in adult mice, with the main decrease occurring between days 10 and 25.

Paralemmin mRNA is readily detectable in the mouse neuroblastoma cell lines NS20Y (Fig. 3, *bottom*, lanes *N*), N1E115, NH15CH2, and 108CC15 (not shown) and also in the mouse fibroblast cell line L929 (Fig. 3, lane *L*). Morphological differentiation of NS20Y cells by serum withdrawal does not notably affect the mRNA abundance (Fig. 3, lanes *N 0.5* vs. *N 10*). To test whether protein kinase–mediated signaling pathways affect paralemmin mRNA expression, as observed for GAP-43 mRNA (Karns et al., 1987), neuroblastoma cells were treated with the cAMP-inducing agents forskolin and IBMX, the calcium ionophor A23187, and the phorbol ester 12-O-tetradecanoylphorbol-13-acetate (TPA), and analyzed by Northern blot hybridization. No significant effects on paralemmin mRNA abundance were seen (see Fig. 3, lanes *N Ca* vs. *N* − for the Ca^{2+} ionophore experiment, other data not shown; experimental details are given in Materials and Methods).

Among the multiple brain cDNA clones analyzed by us, one mouse and one human clone contained a sequence insert (underlined in Figs. 1 and 2). We suspected differential mRNA splicing and investigated this by RT-PCR of different chicken, human, and mouse tissues (Fig. 4). Based on the human paralemmin gene structure (Burwinkel et al., 1998), PCR primers were placed in exons 4 and 9. Agarose gel electrophoresis of RT-PCR products yielded a characteristic band pattern. Sequencing showed that the main bands differ by the presence or absence of exon 8. The bottom-most band only obtained from chicken brain lacks both exons 7 and 8; additional bands (Fig. 4, *asterisks*) are heteroduplexes. The relative expression of mRNAs with and without exon 8 differs between tissues, and this tissue specificity is largely conserved between chicken, mouse, and man. The longer mRNA predominates in most tissues (most prominently and consistently in skeletal muscle, heart, and lung) whereas the shorter mRNA prevails in brain and kidney.

The possibility of differential splicing of exon 4 was probed by RT-PCR of RNA from human brain, kidney, muscle, heart, liver, fibroblasts, and whole blood, with primers in exons 3 and 5, but only one amplification product of expected size and sequence was obtained from all tissues (not shown).

Differential splicing of exon 8 in brain is developmentally regulated. The panel at the bottom of Fig. 4 shows that in newborn mouse brain, the mRNA including exon 8 is hardly detectable. It is induced as the mice grow up, most pronouncedly between postnatal days 10 and 20.

Paralemmin Analyzed by Immunoblotting: Anomalous Electrophoretic Migration, Electrophoretic Heterogeneity, and Tissue Distribution

Fig. 5 *A* shows a Western blot of brain proteins from rat,

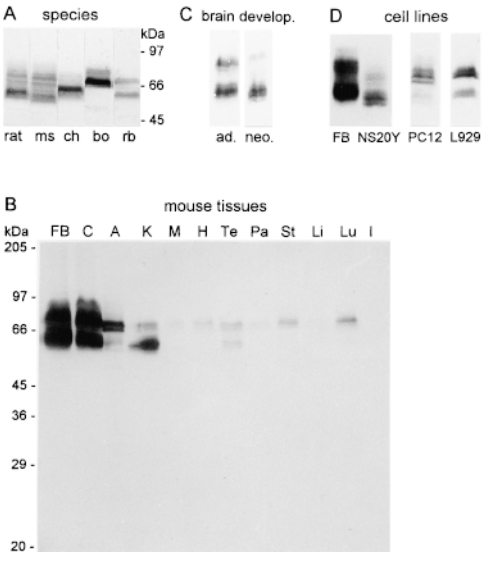

Figure 5. Electrophoretic heterogeneity and tissue distribution of paralemmin in Western blot analysis. (*A*) Brain homogenates from rat, mouse (*ms*), chicken (*ch*), cow (*bo*), and rabbit (*rb*) (30 μg protein per lane). (*B*) Homogenates from mouse tissues (designations as in Fig. 3; 40 μg protein per lane except *A* [160 μg] and *M* [60 μg]). (*C*) Brain homogenates from adult (*ad.*) and neonatal (*neo.*) mouse (10 μg protein). (*D*) Lysates from NS20Y (20 μg), PC12, and L929 cell lines (both, 60 μg) compared with mouse forebrain homogenate (*FB*, 10 μg).

mouse, chicken, cow, and rabbit developed with an antiserum raised against recombinant mouse paralemmin. The blot displays several remarkable features. (*a*) Multiple bands are seen in all five species, spread out over considerable ranges of apparent molecular size. Moreover, the electrophoretic mobilities of these arrays of bands differ considerably between rodents, chicken, cow, and rabbit. (*b*) Band patterns from all species consist of a lower and an upper group, each of which is a series of closely and evenly spaced individual bands. This is most clearly visible in the rodents where the band spacing is widest. (*c*) The lower main bands of mouse and chicken paralemmin have apparent molecular sizes of 60 and 65 kD, respectively, as opposed to a predicted molecular weight of 37.2 kD for paralemmin, without exon 8, in either species. Thus, electrophoretic mobilities are both slower than expected from the primary structures, and differ markedly between paralemmins with the same predicted molecular weights but from different species. (*d*) The same band patterns are observed (not shown) when a Western blot is stained with antiserum raised against a synthetic peptide spanning amino acids 13–27 of mouse paralemmin, indicating that all molecules represented by the electrophoretically distinct bands share this NH_2-terminal part (encoded by exons 2 and 3) of the paralemmin sequence.

Initially, glycosylation was considered as a possible reason for the unexpectedly slow electrophoretic mobility, the band heterogeneity, and the species differences. However, treatment of chicken synaptic plasma membranes with neuraminidase, *N*-glycosidase F and O-glycosidase followed by immunoblotting yielded no effects on the electrophoretic mobility of paralemmin, unlike fetuin as a positive control (data not shown). It appears therefore that the slow electrophoretic mobility is not a reflection of true molecular size but attributable, e.g., to detergent-resistant conformation motifs or to the acidic character of paralemmin, in agreement with similarly retarded electrophoretic mobility of other acidic proteins like amphiphysin, GAP-43, MARCKS, and chromogranins. The remarkable species differences suggest that electrophoretic mobility is very sensitive to small variations in amino acid sequence. Mouse and chicken paralemmins have markedly different mobilities in spite of essentially identical predicted molecular weights and isoelectric points, and bovine paralemmin migrates slower yet although it is probably more similar to mouse than to chicken paralemmin in primary structure.

An immunoblot analysis of homogenates from different mouse tissues is shown in Fig. 5 *B*. Expression of paralemmin protein is distinctly highest in brain, intermediate in adrenal gland and kidney, and much lower or undetectable in the other tissues. This tissue distribution of gene product abundance agrees well with the Northern blot analysis of chicken paralemmin mRNA (Fig. 3) but less so with the human Northern blot. Tissue differences or species differences in the rates of paralemmin mRNA translation may account for the discrepancies. All three Northern and Western blots agree in that brain is the tissue where paralemmin expression is highest.

Fig. 5 *B* also shows that the band patterns differ between tissues. The lower group of bands dominates in kidney and is expressed in similar abundance as the upper group in brain and testis, whereas the upper group dominates in all other tissues. This correlates well with the tissue distribution of the long and short splicing variants of paralemmin mRNA (Fig. 4) suggesting that the the lower group of the Western blot pattern represents the short splicing variant whereas the long splicing variant underlies the upper group of bands. This is further corroborated by the observations that in mouse brain the upper band group is more intense in adult than in neonatal brain (Fig. 5 *C*), as is the longer splicing variant (Fig. 4, *bottom*), and that in chicken brain both the upper band group on Western blots (Figs. 5 *A* and 7 *A*) and the longer splicing variant (Fig. 4, *top*) are very faint. As for the whole protein, the differences between the upper and lower groups in apparent molecular size according to electrophoretic mobility (mouse, 20 kD; chicken, 8 kD) are much larger than the predicted size differences of the differential splicing products (5 kD).

In addition to differential splicing, other forms of molecular heterogeneity of paralemmin appear to exist that are responsible for the fine-structure of the Western blot band patterns evident particularly in the mouse. In nonneural tissues and in L929 fibroblast cells, both the upper and the lower band group each form a doublet, whereas three or more bands per group are seen in forebrain, cerebellum, PC12 cells, and NS20Y cells (Fig. 5). Moreover, in the brain samples, the lowermost bands of each group are very weak so that the whole band pattern is shifted upwards in comparison to nonneural tissues (Fig. 5 *B*) and to cell lines (Fig. 5 *D*). Band fine structure also differs between neonatal and adult mouse brain (Fig. 5 *C*). In conclusion, electrophoretic heterogeneity of paralemmin (presumably reflecting molecular heterogeneity) is higher in brain and neuronal cell lines than in nonneural tissues and cells, and is subject to developmental changes.

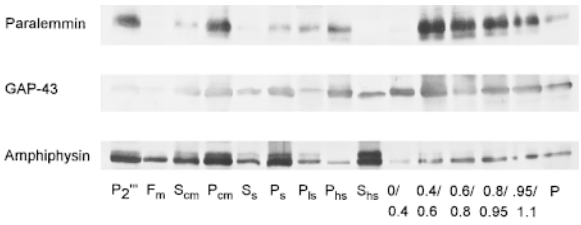

Figure 6. Distribution of paralemmin among subcellular fractions of the purification course of chicken synaptic plasma membranes, in comparison to GAP-43 and amphiphysin. 25 μg of protein from each fraction was analyzed by immunoblotting. Fraction designations are as in Babitch et al. (1976). P_2'', washed 13,600 rpm pellet of brain homogenate ("mitochondrial pellet"). Fractions and subfractions of P_2'' after Ficoll step gradient: F_m, "mitochondrial fraction;" S_{cm} and P_{cm}, "myelin supernatant and pellet;" S_s and P_s, "synaptosomal supernatant and pellet." Fractions and subfractions after hypotonic lysis of P_s synaptosomes: P_{ls}, "intrasynaptosomal mitochondria;" P_{hs}, large membranes; S_{hs}, cytosol and small vesicles. Saccharose step gradient fractions of P_{hs}: *0/0.4*, interface between 0 and 0.4 M saccharose, etc.; *P*, mitochondria-rich pellet. The course of purification of synaptic plasma membranes is P_2''–P_s–P_{hs}; 0.4/0.6/0.8.

Paralemmin Co-distributes with the Plasma Membrane in Cell Fractionation and is Protease-sensitive

Fractions of the purification course of chicken synaptic

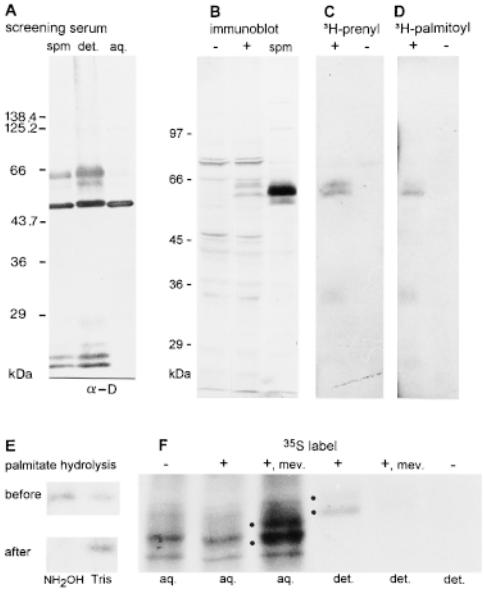

Figure 7. Analysis of paralemmin lipidation. (*A*) Immunoblot of chicken brain synaptic plasma membranes before (*spm*) and after Triton X-114 partitioning into detergent (*det.*) and aqueous (*aq.*) phases, developed with the screening serum (*α-D*) with which the original chicken paralemmin cDNA was isolated. The blot demonstrates that paralemmin (diffuse double band near the 66-kD marker) and GAP-43 (intense band below) are among the main antigens detected by this serum (15 μg protein per lane). (*B*) Immunoblot of COS-7 cell lysates (100 μg protein each) either expressing the chicken paralemmin cDNA (+) or transfected with the corresponding antisense expression plasmid (−), and of chicken brain synaptic plasma membranes (*spm*; 30 μg protein). (*C*) Prenylation of paralemmin, expressed from the chicken cDNA in COS-7 cells, demonstrated by metabolic labeling. Lysates (220 μg protein) of COS-7 cells transfected with chicken paralemmin cDNA in sense (+) or antisense (−) orientation and grown in the presence of [^{3}H]mevalonolactone were subjected to immunoprecipitation with an antiserum against recombinant chicken paralemmin, and the precipitate analyzed by SDS-PAGE and fluorography for 41 d. (*D*) Palmitoylation of paralemmin demonstrated by metabolic labeling with [^{3}H]palmitate. Lysates (220 μg) of COS-7 cells transfected with chicken paralemmin cDNA in sense (+) or antisense (−) orientation and grown in the presence of [^{3}H]palmitate were subjected to immunoprecipitation with an antiserum against recombinant chicken paralemmin, and the precipitate analyzed by SDS-PAGE and fluorography for 41 d. (*E*) Release of paralemmin-bound [^{3}H]palmitate by hydrolysis with hydroxylamine. An SDS gel with immunoprecipitates of [^{3}H]palmitate-labeled paralemmin on two adjacent lanes was prepared as in part *D*. In this experiment, the lower band of the doublet seen in *D* was prominent whereas the upper band was very faint. After fluorography, the gel was re-swollen, cut between the lanes, and the left lane was incubated in 1 M hydroxylamine, pH 7.5, overnight whereas the right lane was control incubated in 1 M Tris, pH 7.5. Subsequently, both parts of the gel were again subjected to fluorography. The period of fluorography before and after hydrolysis was 3 mo each. (*F*) Inhibition of lipidation affects electrophoretic mobility and hydrophobicity of paralemmin. COS-7 cells were transfected with chicken paralemmin cDNA in sense (+) or antisense (−) orientation and grown in the presence of [^{35}S]methionine and cysteine, plus, where indicated, the inhibitor of prenylation, mevinolin (*mev.*). Lysates were immunoprecipitated, and the precipitates were subjected to Triton X-114 phase partitioning. Aqueous (*aq.*) and detergent (*det.*) phases underwent SDS-PAGE followed by fluorography for 9 d. Dots mark positions of paralemmin bands.

plasma membranes were analyzed by immunoblotting for paralemmin and the reference proteins, amphiphysin, and GAP-43 (Fig. 6). Paralemmin is most highly enriched in the fractions of the final sucrose step gradient (0.4/0.6 and 0.6/0.8) that contain the purified synaptic plasma membranes. It co-distributes with the activity of the plasma membrane marker protein, Na/K-ATPase (not shown). The distribution of paralemmin is similar to that of GAP-43, though GAP-43 is found in some quantity also in the lighter fractions S_{hs} and 0/0.4 (supernatant of the synaptosomal lysate and top of the sucrose gradient) in which paralemmin is very low. In contrast, amphiphysin, which is primarily synaptic vesicle–associated and cytoplasmic, is abundant in the light fractions. This distribution was found consistently in two independent synaptic plasma membrane preparations.

In the course of a cell fractionation procedure leading to the purification of synaptic vesicles from chicken brain, paralemmin distribution also follows that of GAP-43 and is distinct from the distribution of the intrinsic synaptic vesicle protein, SV2 (data not shown). In this analysis, we also noted that paralemmin is highly sensitive to endogenous proteases, undergoing rapid degradation to multiple immunopositive bands as soon as protease inhibitors are omitted in the final steps of the fractionation procedure, whereas the control proteins (GAP-43, amphiphysin, and SV2) remained intact. Conserved PEST-like sequences (rich in proline, glutamate, serine, and threonine residues; Rechsteiner and Rogers, 1996) in the paralemmin primary structure (amino acids 92–107 and 271–282 in chicken) may contribute to this protease sensitivity.

COOH-terminal Prenylation and Palmitoylation of Paralemmin Confer Hydrophobicity, Electrophoretic Heterogeneity, and Membrane Attachment

The original paralemmin cDNA, ch10.12.1, was isolated in an immunoscreening with a serum raised against the detergent phase of synaptic plasma membranes, which contains the hydrophobic proteins, and immunoblot analysis of the aqueous and detergent phases shows that paralemmin distributes almost entirely into the latter (Fig. 7 *A*). Paralemmin and GAP-43 are in fact the two main antigens recognized by both screening sera that were raised against the synaptic plasma membrane detergent phase (Fig. 7 *A*). The paralemmin cDNA predicts a highly polar protein without any hydrophobic stretches that could constitute a transmembrane domain, but the COOH terminus carries a combination of three sequence features, highly conserved between mouse, human, and chicken (Fig. 2 *A*), that are known to contribute to the membrane attachment of proteins. A CaaX prenylation consensus motif is immediately preceded by two additional cysteine residues, and cysteines in similar constellations have been shown to be palmitoylated in several other proteins. Upstream of these three cysteines (the only conserved cysteine residues in paralemmin) is a cluster of basic residues; basic clusters have been demonstrated to contribute to the membrane association of several proteins in cooperation with lipid anchors (Hancock et al., 1991; Clarke, 1992; Giannakouros and Magee, 1992; Magee and Newman, 1992; Cadwallader et al., 1994). Fig. 2 *C* aligns the COOH-terminal sequences

of paralemmin with those of Ras isoforms and of a membrane-associated protein from *Xenopus laevis*, xlgv7. The COOH terminus of xlgv7 is particularly similar to that of paralemmin, displaying all three sequence motifs. H-ras and xlgv7, whose sequences are otherwise unrelated to paralemmin, have been demonstrated to be both, farnesylated and palmitoylated (Kloc et al., 1991, 1993; and references therein).

To see whether paralemmin too is prenylated and palmitoylated, we performed metabolic labeling experiments in cell culture. The chicken cDNA, encoding the splicing variant without exon 8, was transiently expressed in COS-7 monkey kidney cells, and an antiserum against the chicken protein that does not recognize mammalian paralemmin was used for immunoprecipitation and immunoblotting. Fig. 7 *B* shows an immunoblot of COS-7 cells transfected with negative control plasmid (−) and chicken paralemmin cDNA (+), along with chicken synaptic plasma membranes (spm) as reference. The single cDNA gives rise to two protein bands, confirming that mechanisms in addition to differential splicing contribute to the band heterogeneity of paralemmin seen on immunoblots of tissues and cell lines. The lower cDNA-derived band comigrates with the lower edge of the main band in chicken synaptic membranes whereas a counterpart of the upper band may be part of the diffuse, broad trail characteristic for chicken brain paralemmin. The lower, weak band of the brain sample has no counterpart in the transfected cells. It probably corresponds to the minor splicing variant of chicken brain that lacks both exons 7 and 8 (Fig. 4). The comigration of recombinant and native paralemmin confirms that the cDNA-deduced amino acid sequence is full-length, and that the anomalously slow migration in SDS-PAGE appears to be an intrinsic property of the polypeptide.

Metabolic labeling for prenylation was performed by incubating transfected cells with the prenyl precursor, [^{3}H]mevalonolactone, in the presence of the inhibitor of endogeneous mevalonate synthesis, mevinolin (Fig. 7 *C*). Palmitoylation was detected by labeling with [^{3}H]palmitate (Fig. 7 *D*). The results show that paralemmin is indeed both prenylated and palmitoylated. With each label, band doublets are obtained that probably correspond to the two bands seen on the Western blot (Fig. 7 *B*). Additional, weak bands of lower molecular size (25 and 35 kD) may be proteolytic degradation products. Prenyl- and palmitoyl-labeled bands seem to comigrate. Labeling with mevalonate does not discriminate between the incorporation of farnesyl and geranylgeranyl residues as it is a precursor for both. However, as the COOH-terminal amino acid of paralemmin is invariably methionine, it is predicted from previous analysis of prenylation consensus sequences (Clarke, 1992; Giannakouros and Magee, 1992) that paralemmin is farnesylated.

To clarify whether palmitoyl incorporation occurs indeed by thioester linkage to the COOH-terminal cysteine residues rather than by ester bonding to serine or threonine residues elsewhere in the protein, [^{3}H]palmitate-labeled paralemmin was incubated either with 1 M hydroxylamine or 1 M Tris at pH 7.5 (Fig. 7 *E*). 1 M hydroxylamine at neutral pH is known to selectively hydrolyze thioester bonds but neither hydroxyesters nor the thioether bonds of prenyl residues. The selective disappearance of the radioactive band in the hydroxylamine-treated lane indicates that palmitate is bound to paralemmin predominantly or exclusively by thioester linkage.

Fig. 7 *F* shows that lipidation affects paralemmin's hydrophobicity and electrophoretic mobility. As it is known that palmitoylation next to prenylation sites depends on previous prenylation, paralemmin was transiently expressed from the chicken cDNA in COS-7 cells in the presence or absence of mevinolin, metabolically labeled with ^{35}S amino acids, and subjected to immunoprecipitation followed by detergent phase partitioning, SDS-PAGE, and fluorography. Immunoprecipitation from the aqueous phases yields a high background of unspecific ^{35}S-labeled bands. Still, it can be seen that from untreated cells (+) a doublet with a strong lower and a weak upper band, similar to the pattern in Fig. 7 *D*, is immunoprecipitated that partitions into the detergent phase. In mevinolin-treated cells (Fig. 7 *F*, +, *mev.*) these bands in the detergent phase are much fainter, whereas two new bands with faster electrophoretic mobility appear in the aqueous phase that cannot be seen in the aqueous phase from untreated cells. This indicates that prenylation and subsequent palmitoylation are responsible for association of paralemmin with the hydrophobic fraction in Triton X-114 phase partitioning. Moreover, it is demonstrated that the course of posttranslational processing (which is presumably initiated by prenylation, followed by removal of the three COOH-terminal amino acids, methylation of the new COOH terminus [Clarke, 1992; Giannakouros and Magee, 1992], and the addition of one or two palmitoyl residues) affects the electrophoretic mobility of paralemmin and produces at least four electrophoretically distinct intermediate and end products.

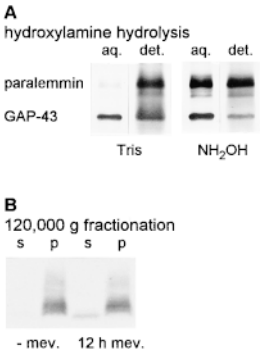

Figure 8. (*A*) Hydroxylamine hydrolysis reduces the hydrophobicity of native paralemmin. Chicken synaptic plasma membranes (130 μg protein) were incubated for 4 h with 1 M hydroxylamine, pH 7.5, or for control, with 1 M Tris, pH 7.5. After Triton X-114 phase partitioning, the aqeous (*aq.*) and detergent (*det.*) phases were subjected to SDS-PAGE and Western blotting, and paralemmin and GAP-43 were simultaneously visualized by development with antiserum α-D (compare with Fig. 7 *A*). (*B*) Paralemmin in undifferentiated NS20Y cells is entirely associated with the 120,000 *g* pellet (*p*), and mevinolin treatment causes the appearance of paralemmin also in the 120,000 *g* supernatant (*s*). NS20Y cells were grown at 10% serum in the absence (*−mev.*) of mevinolin and for 12 h in the presence of 50 μM mevinolin (*12 h mev.*). Cells were homogenized, subjected to 120,000 *g* fractionation, SDS-PAGE and blotting, and then the blot was developed with antibody No. 10 directed against recombinant mouse paralemmin. Cultivation of the cells in the presence of mevinolin for 24 h or longer led to pronounced morphological differentiation, and death and substrate detachment of an increasing number of cells; analysis was therefore terminated after 12 h.

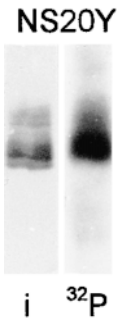

Figure 9. Incorporation of [^{32}P]phosphate into paralemmin by metabolic labeling. NS20Y cells were grown in the presence of [^{32}P]phosphate for 4 h, lysed, and then subjected to immunoprecipitation with rabbit anti–mouse paralemmin serum No. 10, SDS-PAGE, and then blotting onto nitrocellulose. The blot was first exposed to X-ray film for autoradiography (*^{32}P*), and subsequently immunostained (*i*) with chicken anti–mouse paralemmin serum No. HB.

Native paralemmin of chicken synaptic plasma membranes was also subjected to phase-partitioning, with or without previous hydroxylamine treatment (Fig. 8 *A*). The hydroxylamine incubation is expected to hydrolyze the palmitoyl thioester bonds but not the prenyl thioether bonds. GAP-43, which is known to be palmitoylated on Cys-3 and Cys-4, was visualized as an internal control. Without hydroxylamine treatment of synaptic plasma membranes, nearly all of paralemmin and most of GAP-43 distributes into the detergent phase. After hydroxylamine treatment, approximately half of paralemmin and most of GAP-43 goes into the aqueous phase. A similar shift from the detergent to the aqueous phase upon hydroxylamine treatment is seen with paralemmin from mouse L929 fibroblast cells (not shown). These findings indicate that paralemmin of synaptic plasma membranes and fibroblast cells in vivo contains thioester-linked palmitate and that this accounts partially but not completely for the protein's hydrophobic properties.

To test whether lipidation is responsible for the membrane association of paralemmin, we subjected undifferentiated NS20Y cells to 120,000 *g* fractionation before and after mevinolin treatment (Fig. 8 *B*). Before mevinolin treatment, paralemmin is found almost entirely in the pellet whereas after 12 h growth in the presence of mevinolin, a notable quantity of paralemmin appears in the cytosolic fraction. On the blot, it forms a sharp band of high electrophoretic mobility. Apparently, pre-existing paralemmin remains lipidated and membrane attached (prenylation is believed to be irreversible) whereas paralemmin newly synthesized in the presence of mevinolin is unlipidated, electrophoretically more homogeneous, and cytosolic.

The finding that paralemmin of undifferentiated NS20Y cells distributes almost entirely into the 120,000 *g* pellet is notable because immunofluorescence microscopy (see Fig. 11) indicates that paralemmin staining in these cells is to a large part intracellular. This suggests that also intracellular paralemmin in undifferentiated NS20Y cells is associated with a structure that sediments at 120,000 *g*. As paralemmin in these cells also partitions nearly completely into the hydrophobic Triton X-114 phase (not shown), this structure is probably an intracellular membrane compartment.

Paralemmin Is Phosphorylated

The chicken, human, and mouse paralemmin sequences contain several conserved consensus sites for potential phosphorylation by protein kinases A and C, casein kinases I and II, proline-directed protein kinases, and also for tyrosine phosphorylation (Fig. 2 *A*). We therefore investigated whether paralemmin is indeed subject to phosphorylation, by metabolic labeling of endogenous paralemmin of NS20Y neuroblastoma cells with [^{32}P]phosphate

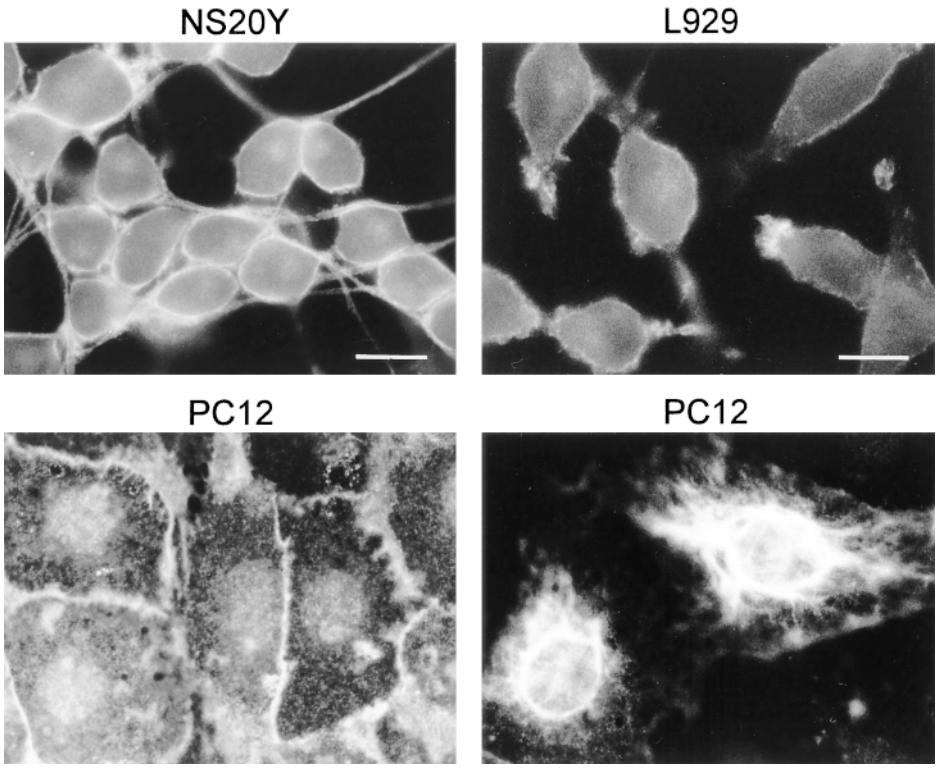

Figure 10. Subcellular distribution of endogenous paralemmin visualized by immunofluorescence microscopy in differentiated NS20Y neuroblastoma cells, L929 fibroblast cells, and PC12 pheochromocytoma cells. The PC12 cells at bottom right represent the subset of cells displaying the very intense staining of a perinuclear, reticular structure; photographic exposure of this image was shorter than at the left where the plasmalemmal and granular intracellular staining exhibited by all PC12 cells is seen. Bars: (*NS20Y* and *PC12*) 15 μm; (*L929*) 9.4 μm.

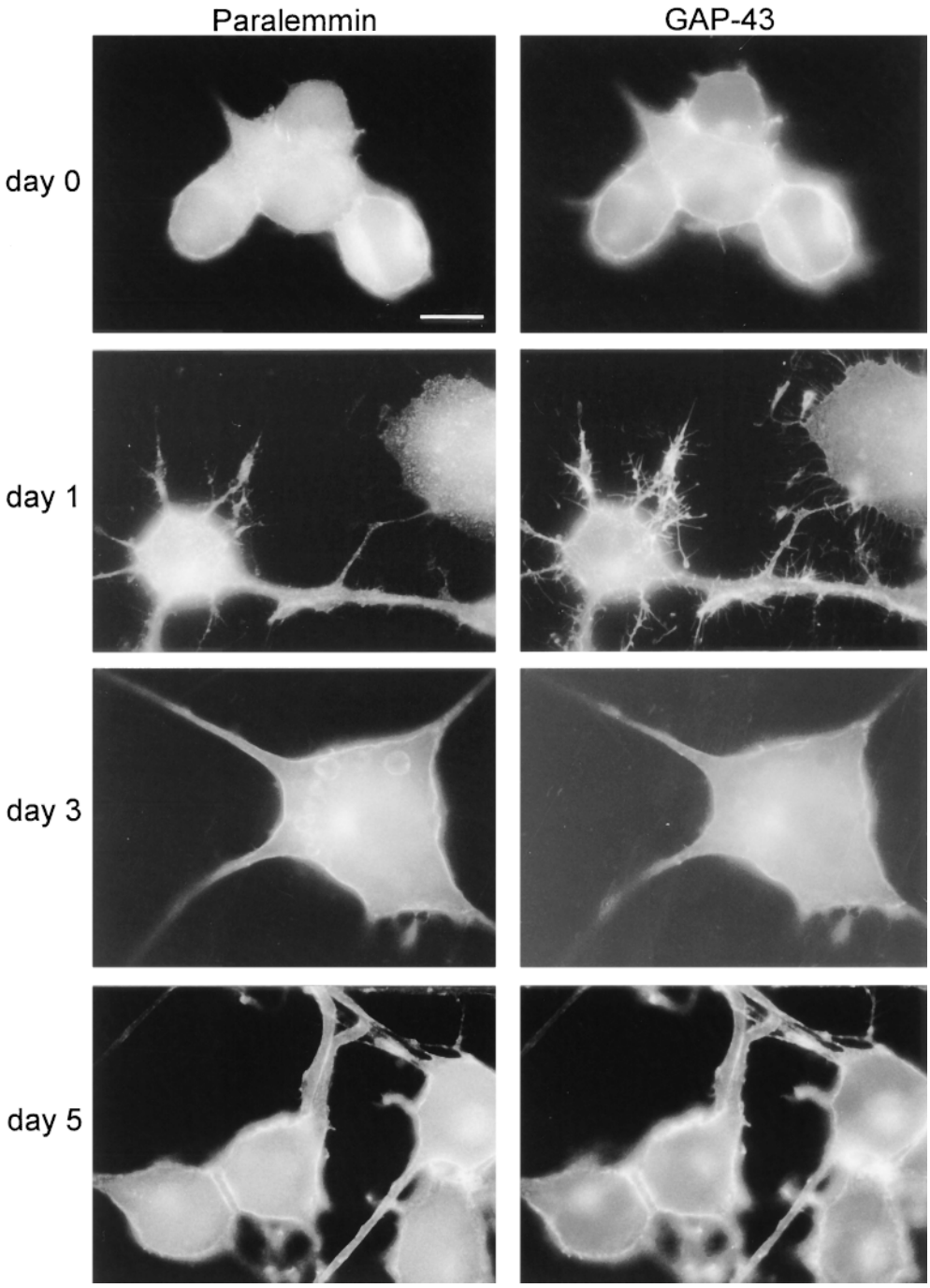

Figure 11. Redistribution of paralemmin and GAP-43 toward the periphery of NS20Y cells in the course of morphological differentiation induced by serum withdrawal. Cells typical for the different stages are visualized by double-immunofluorescence. Bar, 15 μm.

followed by immunoprecipitation and Western blotting. Nitrocellulose blots were analyzed both by immunostaining with anti-paralemmin antibody and by autoradiography. Fig. 9 shows that the array of immunopositive bands is labeled with ^{32}P, with the notable exception of the lowermost band. This suggests that either the paralemmin variant represented by this band cannot be phosphorylated (e.g., lipidation might be a prerequisite of phosphorylation), or that phosphate incorporation leads to an upward band-shift and thus contributes to the electrophoretic heterogeneity of paralemmin.

Immunofluorescence Microscopy of Paralemmin in Cell Culture

Affinity-purified antisera against recombinant mouse paralemmin were used to visualize the subcellular localization of paralemmin. Immunofluorescence microscopy of NS20Y mouse neuroblastoma cells, induced to differentiation by serum withdrawal, shows that immunopositive material appears to be associated primarily with the plasma membrane (Fig. 10; see also Fig. 11). The fluorescence signal outlines the entire periphery of cells and

gives thick processes a tube-like appearance. A more intense signal is often observed in places where cells come close to each other. When the apical or basal regions of cells are in the plane of focus, it can be seen that also fine processes and cell surface blebs are labeled. In addition, a diffuse perinuclear stain is typically seen. N1E-115 mouse neuroblastoma cells yield the same picture (not shown). L929 mouse fibroblastoid cells also display staining of the plasma membrane and of cell extensions. Often, structures at the poles of these characteristically spindle-shaped cells give a particularly strong fluorescence signal (Fig. 10). PC12 pheochromocytoma cells display, in addition to staining of the cell periphery, pronounced labeling of coarsely granular intracellular structures (Fig. 10, *bottom left*). About 30% of the PC12 cells additionally display very intense staining of reticular structures embracing the nuclei and sometimes extending into cell processes (Fig. 10, *bottom right*; shorter exposure than *bottom left*).

In exploratory double-immunofluorescence experiments comparing the subcellular localization of paralemmin in differentiated NS20Y cells to several marker proteins, we noted a high degree of colocalization with GAP-43. Because of the role of this protein in cell process formation, we compared the localization of paralemmin and GAP-43 during morphological differentiation of the NS20Y cells by serum withdrawal (Fig. 11). A shift of paralemmin from the cytoplasm to the plasma membrane

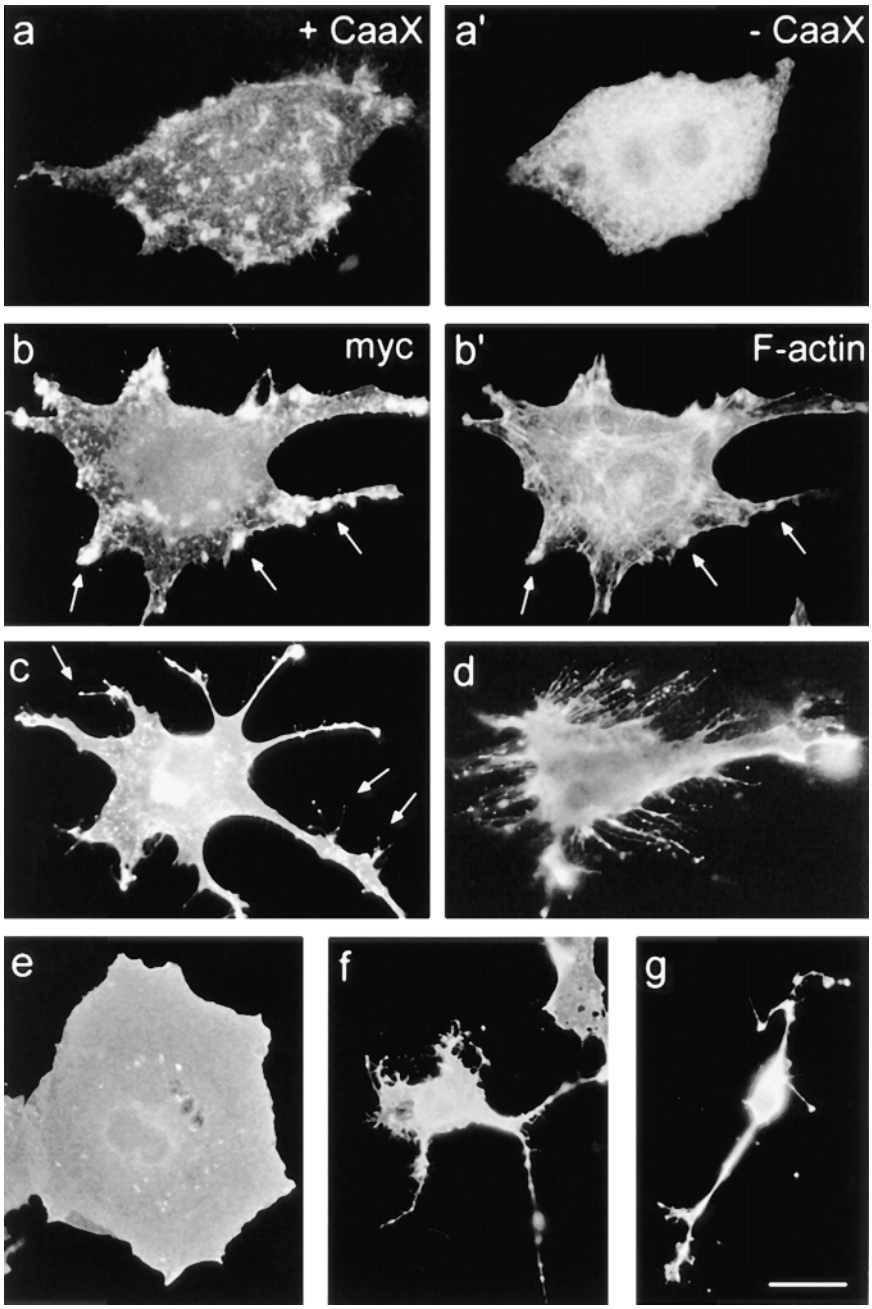

Figure 12. Characteristic aspects of the morphology of paralemmin overexpressing cells. (*a*, *a′*) +CaaX paralemmin is targeted to the plasmalemma where it concentrates at membrane protuberances, whereas −CaaX paralemmin is cytoplasmic (PC12 cells, immunolabeling with anti-myc). (*b*, *b′*) Double-fluorescent labeling of a +CaaX-transfected L929 cell for recombinant paralemmin (anti-myc) and F-actin (phalloidin). Paralemmin concentrates in membrane prominences like filopodia and microspike clusters, many of which are also labeled for F-actin (*arrows*). The cell has a well-structured stress fiber skeleton qualitatively indistinguishable from neighboring non-overexpressing cells of similar shape (not shown). (*c*) Dendritic L929 cell after +CaaX paralemmin transfection with labeling of plasma membrane protuberances including filopodia (*arrows*). Note the bright labeling of filopodial tips (anti-myc). (*d*) +CaaX paralemmin–expressing GM5756t cell featuring many long filopodia. Note the dotted pattern of paralemmin along and at the tips of filopodia (anti-paralemmin labeling). (*e*) COS-7 cell representing the broadly expanded early stage under +CaaX paralemmin expression, featuring a very flat cell shape and relatively smooth edges and surface (*e–g*, anti-paralemmin labeling). (*f*) COS-7 cell representing the partially collapsed later stage under +CaaX paralemmin expression, featuring a small but still flat perikaryal area displaying filopodial and lamellipodial membrane activity, and several long thin extensions carrying multiple varicosities. (*g*) COS-7 cell representing the late stage under +CaaX paralemmin expression, featuring a highly condensed cell body extending few, cable-like processes with varicosities but little membrane activity. Note that all three COS-7 cell types (*e–g*) are of equal magnification. Bar: (*a–d*) 2.5 μm; (*e–g*) 3.8 μm.

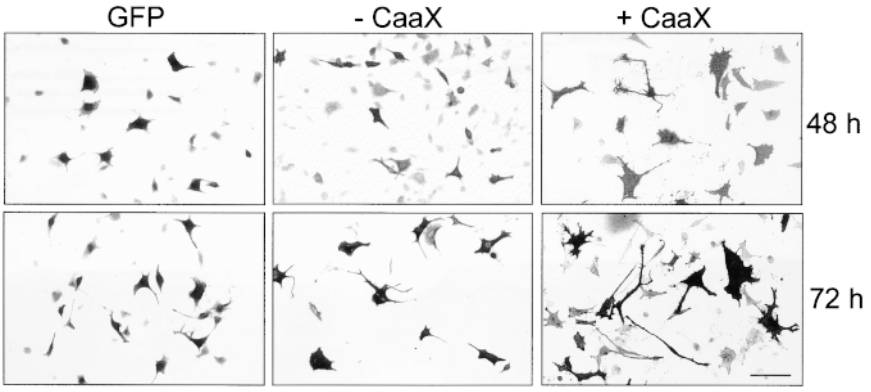

Figure 13. Overexpression of lipid-anchored paralemmin (+*CaaX*) but not of anchorless paralemmin (−*CaaX*) induces spreading and process formation in L929 fibroblasts. Typical fluorescence micrographs are shown of cells 48 and 72 h after transfection with the respective paralemmin constructs or with pEGFP-C1 (*GFP*) as negative control. Photographic negatives are shown for better reproduction of fine detail. GFP is visualized by its intrinsic fluorescence, and paralemmin with anti-paralemmin immunofluorescence. Note the background of weakly immunofluorescent cells that are either untransfected or low expressing transfected cells, illustrating the relative abundances of endogenous versus overexpressed recombinant paralemmin in this experimental system. The GFP and −CaaX images display the intrinsic tendency of L929 cells to spread and form processes during 3 d in culture that is grossly exaggerated by +CaaX paralemmin overexpression. Bar, 11 μm.

in the course of this process was observed. Before serum withdrawal (day 0), much of paralemmin appears to be intracellular, with little highlighting of the cell periphery. Paralemmin-immunofluorescence in the cytoplasm often has a finely granular or vesicular appearance. GAP-43, at this stage, is already more peripherally localized, with the plasma membrane outlined more distinctly, and labeling of fine and occasional short thick processes that are paralemmin-negative. Upon serum withdrawal, the cells form neurite-like long extensions in the course of 7 d. Concurrently, both paralemmin and GAP-43 translocate towards the plasma membrane and towards the ends of processes. However, GAP-43 does so faster and more markedly, labeling many fine ramifications of the long processes at days 1 and 3, apparently concurrent with their formation. In contrast, paralemmin still is largely cytoplasmic at day 1, often with distinct vesicular or granular appearance, and it also enters the neurite-like processes at days 1 and 3 but does not label their terminal ramifications as sharply as GAP-43. At days 5 and 7 the translocation of both proteins is finished and they give a very similar appearance in immunofluorescence. They now label the circumference of the cell body, the fine processes extending directly from the cell body, and the trunks and main branches of long processes. GAP-43 has apparently withdrawn from the terminal ramifications of long processes that it so strongly labeled during their formation.

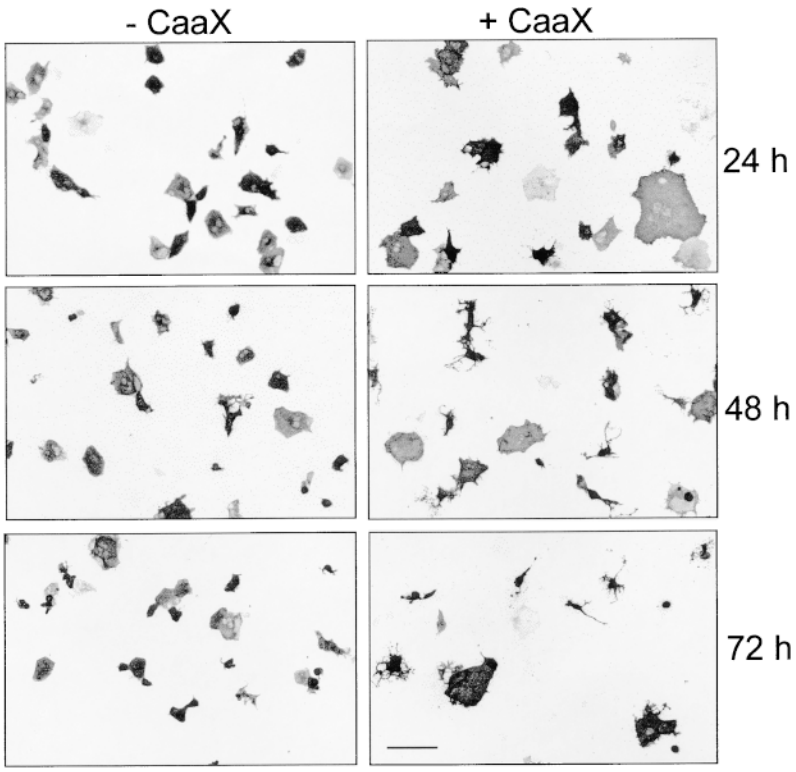

Figure 14. Overexpression of lipid-anchored paralemmin (+*CaaX*) but not of anchorless paralemmin (−*CaaX*) induces spreading and subsequent collapse of COS-7 cells. Typical fluorescence micrographs are shown of cells 24, 48, and 72 h after transfection with the respective paralemmin constructs. Photographic negatives are shown for better reproduction of fine detail. Control cells transfected in parallel with pEGFP-C1 (not shown) displayed shapes indistinguishable from the −CaaX-transfected cells at the respective time points. Recombinant paralemmin is visualized by immunofluorescence with the myc tag antibody. Bar, 15 μm.

Overexpression of Paralemmin Induces Cell Expansion and Process Formation

The molecular properties and subcellular localization of paralemmin made us suspect an involvement in plasma membrane dynamics and/or membrane–cytoskeleton interaction. Plasmids expressing the long splicing variant of paralemmin including exon 8, tagged with a myc epitope at the NH_2 terminus and either including or lacking the COOH-terminal 15 amino acids assumed to be responsible for lipidation-mediated membrane anchoring, were transfected into several cell lines for transient expression under the control of the strong CMV promoter. By double-immunofluorescence microscopy with paralemmin and myc antibodies, paralemmin levels in transfected cells were estimated to be severalfold higher than endogenous paralemmin in neighboring untransfected cells (see Fig. 13).

Full-length recombinant paralemmin was found to associate with the plasma membrane in all investigated cell lines, and to concentrate particularly at sites of membrane activity such as microspike clusters, filopodia and process tips (Fig. 12). The COOH-terminally truncated protein, in contrast, accumulated in the cytoplasm, excluding the nucleus and intracytoplasmic vacuoles, demonstrating that the COOH-terminal lipidation motif is essential for anchoring this protein to the plasma membrane (Fig. 12 *a′*). At highest magnification, anchorless paralemmin gives a punctate staining, suggesting that it associates with particulate or vesicular structures in the cytoplasm.

Overexpression of membrane-anchored paralemmin induced conspicuous changes of cell shape over a time course of one to three days. Paralemmin-transfected L929 fibroblasts grow very wide and flat and/or extend long processes (Figs. 12 *c* and 13). Stellate and bizarre, segmented morphologies develop later on. In contrast, L929 cells transfected with paralemmin lacking the lipid anchor remain similar to the untransfected cells surrounding them and to control cells transfected with GFP, all three cell groups typically flattening and producing few short processes during 3 d in culture (Fig. 13).

Human GM5756t fibroblasts transfected with full-length paralemmin are also induced to expand and develop bizarre shapes with jagged processes whereas GM5756t cells transfected with paralemmin lacking the membrane anchor remain more slender, similar to the typical fibroblast shape of untransfected cells (not shown).

Untransfected and GFP-transfected COS-7 cells are flat, round, or polygonal cells or have a fibroblastoid shape. Transfected with full-length paralemmin (Figs. 12, *e–g*, and 14, *+CaaX*), they grow very wide and flat within the first day. Many subsequently appear to collapse or re-organize into compact perikarya with long and thin, cable-shaped processes that are sometimes highly branched, so that the cell population becomes very polymorphic after 2 and 3 d (Fig. 14). In contrast, COS-7 cells transfected with anchorless paralemmin (−CaaX) develop no striking changes of gross morphology. If at all, they shrink rather than expand during the same time interval. Ruffles and lamellipodia are, on the average, more frequent and pronounced on +CaaX cells than on −CaaX cells (see Fig. 12 *f*).

The F-actin cytoskeleton of cells was visualized by fluorescent-labeled phalloidin. Neither full-length nor anchorless paralemmin elicited significant effects on gross cytoskeletal organization, in L929 or COS-7 cells. Stress fiber scaffolds and cortical actin layers were indistinguishable from non-overexpressing neighboring cells of similar shape. Plasma membrane protuberances staining intensely for paralemmin in +CaaX-expressing cells were often also enriched for F-actin (Fig. 12, *b* and *b′*, *arrows*).

PC12 cells displayed the characteristic subcellular localizations of +CaaX and −CaaX paralemmin (Fig. 12, *a* and *a′*) but developed no striking morphological changes, under the expression of neither of the two constructs.

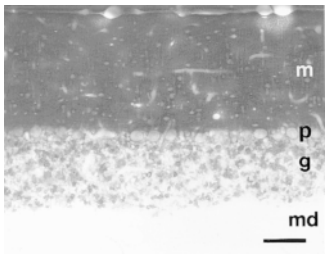

Figure 15. Immunocytochemical visualization of paralemmin in rat cerebellum. *m*, molecular layer; *p*, Purkinje cell layer; *g*, granule cell layer; *md*, medulla. Bar, 72 μm.

Immunocytochemical Localization of Paralemmin in Rat Brain

As paralemmin is most highly expressed in brain and was initially identified as a component of synaptic plasma membranes, we performed an immunocytochemical analysis of rat brain at light and electron microscopic resolution. Paralemmin-like immunoreactivity is expressed in many brain areas. Intense staining is characteristic for neuropil-rich areas wheras myelin fiber–rich regions are spared. The cytoplasm of neuronal cell bodies is only faintly stained. In the cerebellar cortex, for example (Fig. 15), the molecular layer exhibits strong and homogeneous staining, the Purkinje cell somata are only slightly stained and the granule cell layer exhibits a pattern of immunopositive patches, whereas the medulla is essentially unstained.

By immunoelectron microscopy, immunoreaction product is seen in focal aggregates in the perikarya and proximal dendrites of Purkinje cells, either in the cytoplasm or in association with the inner face of the plasma membrane (Fig. 16 *A*). In the molecular layer, the cross-sectioned closely packed bundles of unmyelinated axons localized between the Purkinje cell dendrites, presumably parallel fibers, display a mosaic of strongly stained, moderately stained and unstained fibers (Fig. 16, *A* and *B*). In longitudinally sectioned areas the parallel fibers are sometimes stained at intervals, suggesting a discontinuous distribution of the antigen along the axis of cell processes (Fig. 16 *C*). However, longitudinally sectioned fibers that were immunonegative for long distances were also observed. In Fig. 16 *C*, an immunonegative synapse contacts an immunopositive dendritic spine (*arrow*), presumably an axonal terminal of a parallel fiber contacting a dendritic spine of a Purkinje cell.

The patchy immunopositive structures in the granule cell layer seen by light microscopy (Fig. 15) have a dark periphery and a lighter center at high magnification, and are identified as mossy fiber glomeruli in electron micros-

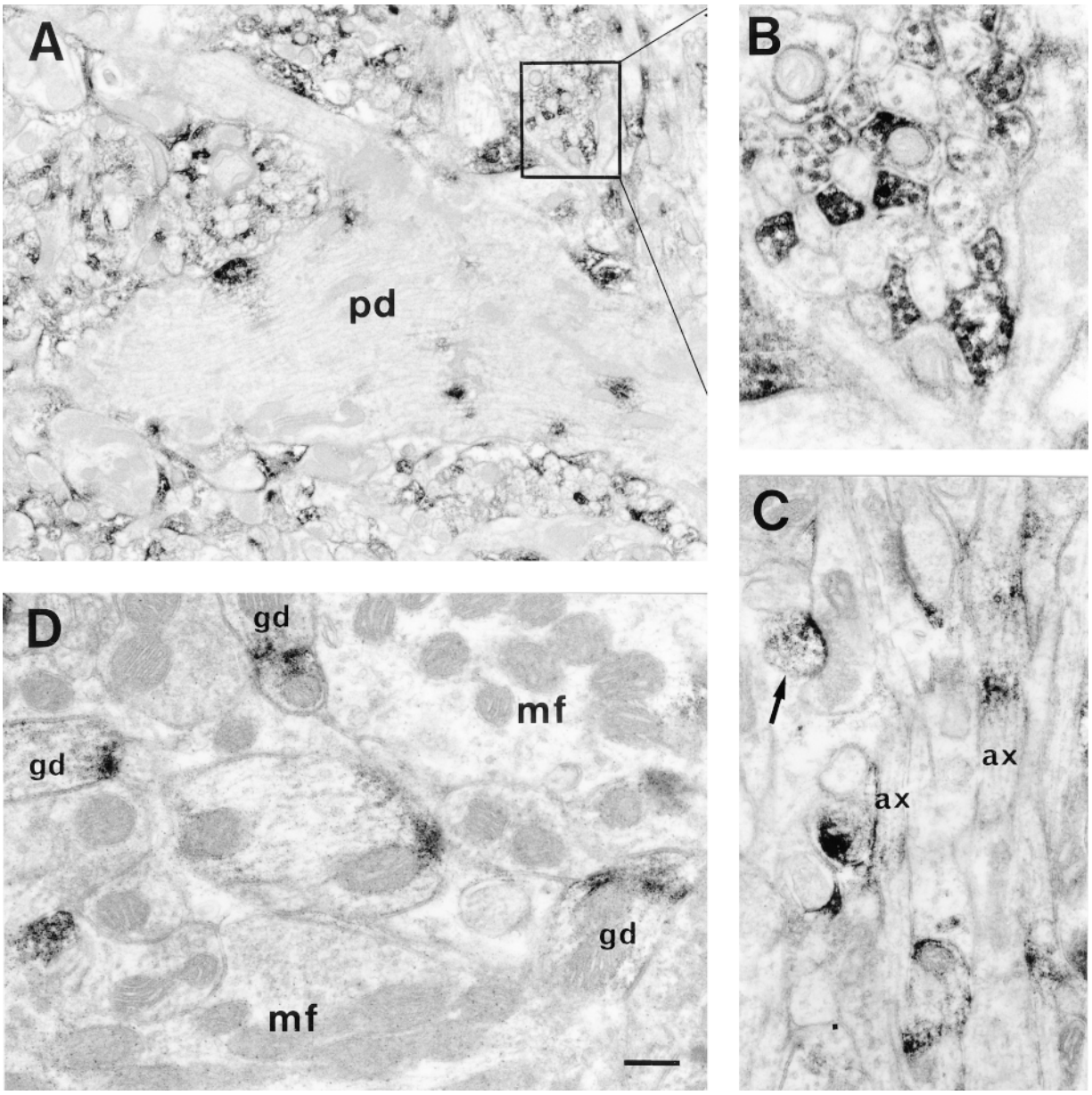

Figure 16. Immunoelectron micrographs of paralemmin-positive structures in the rat cerebellar cortex. (*A*) The thick proximal Purkinje cell dendrite (*pd*) in the molecular layer contains several patches of immunoreaction product and is surrounded by many smaller, heterogeneously stained cell processes, most of them cross-sectioned parallel fibers (magnification shown in *B*). (*C*) Longitudinally sectioned parallel fibers (*ax*) exhibit a discontinuous distribution of immunoreaction product. An immunonegative axonal terminal contacts a positive Purkinje cell spine (*arrow*). (*D*) In the granule cell layer, immunonegative mossy fiber terminals (*mf*) are surrounded by several immunopositive granule cell dendrites (*gd*) showing aggregates of immunoreaction product associated with the plasma membrane. Bar: (*A*) 750 nm; (*B*) 200 nm; (*C*) 400 nm; (*D*) 300 nm.

copy. Paralemmin-negative mossy fiber terminals are surrounded by numerous granule cell dendrites exhibiting plasmalemma-apposed aggregates of reaction product (Fig. 16 *D*). Occasionally, patches of immunopositive material are also observed on the presynaptic side (not shown), but this is less common.

Discussion

We initially identified paralemmin as a new constituent protein of synaptic plasma membranes. Immunoelectron microscopy indicates that, at synapses, it is primarily associated with the postsynaptic plasma membrane. It is not restricted to synapses, though, but is found apparently throughout the inner face of the neuronal plasma membrane and also in association with a particulate or vesicular intracellular compartment. Paralemmin is also expressed in many other tissues and cell types, but the distinctly highest levels of the protein are found in the brain, and within the brain, in neuropil-rich regions.

Several molecular and immunomorphological features of paralemmin are reminiscent of the proteins, GAP-43, CAP-23, MARCKS, and MacMARCKS. Like these, paralemmin is an acidic, highly hydrophilic phosphoprotein attached to the plasma membrane through a lipid anchor, and it lines the membrane surface not uniformly but displays a focal distribution (for paralemmin, evident only in electron microscopy). A direct comparison of the subcellular localization and dynamics of paralemmin and GAP-43 in differentiating neuroblastoma cells by doubleimunofluorescence microscopy revealed a high degree of similarity but also subtle differences (Fig. 11). There is no explicit sequence similarity among paralemmin, GAP-43, CAP-23, and MARCKS, and the latter three proteins have been implicated in a variety of cell biological functions such as formation of cell processes (Zuber et al., 1989; Aigner et al., 1995; Caroni et al., 1997; Aarts et al., 1998), phagocytosis (Allen and Aderem, 1995), exocytosis (Dekker et al., 1989; Gamby et al., 1996*a*), or in signal transduction (Strittmatter et al., 1993, 1995; Gamby et al., 1996*b*). A very general common denominator of GAP-43, CAP-23, and MARCKS seems to be an involvement in events of rapid plasma membrane dynamics (Wiederkehr et al., 1997).

These similarities prompted us to investigate a possible role of paralemmin in the control of cell shape by overexpressing it in several cell lines. In non-neuronal L929, COS-7, and GM5756t cells the overexpression of full-length paralemmin produces conspicuous effects on gross morphology in the course of 1–3 d after transfection. All three cell types profoundly expand their periphery. In addition to spreading, L929 cells emit long processes and often develop grotesque multilobar shapes. GM5756t cells spread and form many short processes. The initial effect on COS-7 cells is broad circumferential spreading, whereas the cell processes evident on many transfected COS-7 cells later on seem to result mainly from secondary collapse or re-organization of the lamellar cell periphery in-between (Fig. 12, *e–g*). These observations are remarkably similar to the long-term effects of GAP-43 overexpression on the gross morphology of non-neuronal cells, which include cell surface expansion, formation of long processes, and collapse of the most highly expressing cells (Verhaagen et al., 1994; Gamby et al., 1996*a,b*; Wiederkehr et al., 1997). The morphogenic effects of both, paralemmin (this work) and GAP-43 (Widmer and Caroni, 1993; Strittmatter et al., 1994; Aarts et al., 1998), depend on an intact lipidation motif to provide membrane anchoring.

We did not observe similarly significant effects of paralemmin overexpression on the overall morphology of the neuronal cell line, PC12. If anything, there may be an increase of thin, short processes. Conceivably, PC12 cells possess stronger mechanisms tethering the "expansive" activity of paralemmin than do the non-neuronal cells, and higher paralemmin expression levels or additional neuritogenic stimuli would be needed to overcome them. Remarkably, also GAP-43 overexpression was found to be insufficient to trigger process formation in PC12 cells by itself, but it potentiated neurite extension stimulated by nerve growth factor (Yankner et al., 1990).

Overexpression of anchorless paralemmin might be anticipated to oppose the action of the endogenous protein by competing for binding partners. We did not see a striking phenotype under −CaaX paralemmin expression though it appeared in some experiments that the number of shrunken or pycnic cells was indeed higher than among GFP control cells. More experiments will be needed to clarify this.

Most studies of the morphogenic activity of GAP-43 have focused on small-scale, rapid plasma membrane dynamics such as filopodial activity and blebbing, that occur on a time scale of minutes to hours. Though we have not systematically investigated such events, paralemmin is likely also to stimulate rapid plasma membrane activity. Filopodia, clusters of microspikes, and other small cell surface prominences are highlighted by immunofluorescence of +CaaX-paralemmin–expressing cells (see Fig. 12). The tips of filopodia are particularly brightly labeled (Fig. 12, *c* and *d*), suggesting that paralemmin concentrates at adhesion complexes, and the vicinity of filopodially active cells is often littered with paralemmin-positive adhesion complex remnants (Fig. 12, *f* and *g*); interestingly, very similar observations have been made with GAP-43 in GAP-43–overexpressing fibroblasts (Aarts et al., 1998). Hovever, as these very fine processes are labeled much more clearly by plasmalemma-associated full-length paralemmin than by cytoplasmic anchorless paralemmin, more systematic studies using a neutral plasma membrane marker for the visualization of these small structures will be needed to clarify whether they are indeed more numerous or longer on +CaaX-paralemmin–transfected cells. In any case, enhanced short-term plasma membrane activity must be supposed to occur as a prerequisite of the observed long-term effects of paralemmin on cell shape, and may now be investigated in more detail in direct comparison with GAP-43, MARCKS, and relatives.

GAP-43 and MARCKS colocalize with F-actin at sites of membrane activity (Widmer and Caroni, 1993; Wiederkehr et al., 1997; Allen and Aderem, 1995), bind actin directly (Hartwig et al., 1992; Hens et al., 1993), and overexpression of GAP-43 leads to the dissolution of stress fibers and the accumulation of monomeric and filamentous actin at GAP-43–induced membrane prominences (Wiederkehr et al., 1997). We also find that many of the cell prominences immunopositive for recombinant paralemmin stain for F-actin, but given the established role of actin in cell surface activity this is not surprising and does not imply a direct interaction of the two proteins. The gross structure of the microfilament cytoskeleton is not notably affected, neither by full length nor by anchorless paralemmin, even at the highest levels of expression. Stress fiber scaffolds and layers of cortical F-actin were typically indistinguishable from those of neighboring untransfected L929 or COS-7 cells with similar morphologies. Flat COS-7 cells 1–2 d after transfection with full-length paralemmin often displayed fewer and thinner stress fibers. This probably reflects the circumstance that these cells are rapidly expanding and likewise need not imply a direct mechanistic link between paralemmin and actin.

The observed morphogenic effects of paralemmin, together with the molecular and immunomorphological similarities, suggest that it might indeed be grouped with GAP-43, CAP-23, MARCKS, and MacMARCKS (a par-

tial homologue of MARCKS) to constitute a broadly defined family of lipid-anchored, acidic phosphoproteins involved in the control of plasma membrane dynamics. Notably, cDNAs of GAP-43, CAP-23, and MARCKS were also picked up in our immunoscreen together with paralemmin (see Introduction), suggesting that they all copurify with synaptic plasma membranes and are strong immunogens. Little is known yet about the molecular mechanisms through which these other proteins work, though functional links, e.g., between GAP-43, the actin cytoskeleton, and signaling proteins (PKC, calmodulin, heterotrimeric [G_o, G_i], and small G proteins [Rho; Aarts et al., 1998]) have been identified.

Membrane expansion requires the insertion of additional membrane surface and the advance and reinforcement of the supporting cytoskeleton. At present, we therefore envision possible mechanistic roles for paralemmin primarily in membrane flow or in membrane–cytoskeleton interaction, although roles such as in signal transmission or in the clustering of other membrane proteins also remain possible.

Coiled-coil interactions between v- and t-SNARES have recently emerged as a crucial mechanism in membrane fusion (Ryan, 1998; Weber et al., 1998), and the NH_2-terminal region of paralemmin with high coiled-coil potential may reflect a function as a t-SNARE that mediates the insertion of intracellular membrane vesicles at sites of plasma membrane expansion. In this context, the similarity of a short sequence tract between paralemmin and Ykt6p, a SNARE of the VAMP/synaptobrevin family involved in ER–Golgi transport in yeast that is also membrane-anchored through a COOH-terminal CaaX motif (McNew et al., 1997), is intriguing, but it remains to be seen whether this is meaningful. Paralemmin is also associated with an intracellular compartment that is sedimentable at 120,000 *g* and probably vesicular, and that translocates partially to the plasma membrane during neuronal differentiation of NS20Y cells (Fig. 11). Intracellular patches of paralemmin immunoreactivity are also seen in immunoelectron microscopy of neuronal perikarya and dendrites (Fig. 16 *A*). Vesicle-associated intracellular paralemmin may simply be en route to its final destination on the plasmalemma, but it might also serve an active role in vesicle trafficking. In this context, it may be significant that vesicular/granular intracellular paralemmin is particularly visible in PC12 neuroendocrine cells (Fig. 10) and adrenal chromaffin cells (not shown).

The interaction between the plasma membrane and the underlying cytomatrix must be loosened at sites of vesicle approach and docking, whereas cytoskeletal structures must be assembled and anchored underneath recently inserted membrane areas. The focal distribution of paralemmin along the plasma membrane may reflect a function in the anchoring of the cortical cytoskeleton. Such anchoring would be crucial for the formation of stable, long cell processes as in paralemmin-transfected L929 cells and, importantly, in the nervous system. On the other hand, the apparent collapse of flat membrane areas after initial radial expansion of COS-7 cells would suggest a more dynamic role, where paralemmin would "drive" membrane insertion to the point of overstretch where subsequent cytoskeletal stabilization by other mechanisms cannot keep pace. Roles in loosening membrane–cytoskeleton interaction have been proposed for GAP-43, CAP-23, and MARCKS (Wiederkehr et al., 1997).

Paralemmin, GAP-43, CAP-23, and MARCKS are coexpressed in neurons and may, in different proportions at different subcellular sites, cooperate in controlling plasma membrane plasticity versus stability. Whereas GAP-43 is specific for neurons and glia, the other proteins are expressed in many cell types but at particularly high abundance in neurons. GAP-43 is concentrated in growth cones, axons, and synaptic terminals (Gorgels et al., 1989; van Lookeren Campagne et al., 1990), whereas MARCKS is also found in dendrites and glial processes (Ouimet et al., 1990). Postsynaptic spines, a prominent site of paralemmin localization, require strong and regulated membrane–cytoskeleton interactions both for the maintenance and the active remodeling of their plasma membrane architecture, e.g., in the interplay with the presynaptic membrane (Hagler and Goda, 1998) or for rapid actin-dependent shape changes (Fischer et al., 1998).

In the animal organism, the main effects of a lack or overexpression of GAP-43, CAP-23, or MARCKS are in nervous system morphogenesis. Overexpression of GAP-43 or CAP-23 results in enhanced axonal sprouting (Aigner et al., 1995; Holtmaat et al., 1995; Caroni et al., 1997), whereas in GAP-43 knockout mice axons are still capable of outgrowth but display pathfinding defects (Strittmatter et al., 1995). Ablation of the MARCKS gene causes extensive abnormalities in brain development (Stumpo et al., 1995). The consequences of paralemmin elimination or overexpression in animals remain to be determined. To search for paralemmin mutations, the chromosomal localization of the paralemmin gene, *PALM*, has been determined in mouse (chromosome 10) and man (19p13.3) (Burwinkel et al., 1998). A protein involved in cell process formation may cause a neurological phenotype but also, e.g., pigmentation defects (compare with the myosin V mutations: Mercer et al., 1991; Pastural et al., 1997). The *grizzled*, *mocha*, *jittery*, and *hesitant* mouse mutations map to the immediate vicinity of the *Palm* gene and display such phenotypes, and the paralemmin coding sequences in these mice have been analyzed but found normal (Burwinkel et al., 1998).

Comparison of the paralemmin sequences from three animal species divides the protein into several circumscript conserved sequence regions that probably represent functional domains, and it will be of obvious interest to analyze these domains and particularly the differentially spliced sequence for their contributions to morphogenic activity and to search for interacting proteins. Immunoblotting reveals considerable molecular heterogeneity of paralemmin, most strikingly in the brain where it is also subject to developmental regulation. Beside differential mRNA splicing, different degrees of phosphorylation and lipidation may contribute to this heterogeneity. There may be yet additional forms of molecular diversity of paralemmin, because by combined treatment with alkaline phosphatase and hydroxylamine we could only partially reduce but not abolish band heterogeneity (data not shown). Differential splicing, on the other hand, seems to be limited to exon 8 as RT-PCR experiments between exons 3 and 9 failed to detect other splice products in multiple tissues,

and immunoblotting with an antibody against an NH_2-terminal peptide encoded by exons 2 and 3 labeled the same set of bands as an antibody against a sequence reaching from exons 2 to 9 (see Results). Cells, and particularly neurons, seem to use multiple molecular variants of paralemmin to fine-adjust the properties through which this protein contributes, apparently, to the control of cell shape.

We thank H.-W. Habbes for excellent technical assistance; Drs. K.M. Buckley, A.I. Magee, P. Wahle, G. Dodt, and R. Paddenberg for reagents and advice; and Ms. U. Neubacher and Prof. U. Eysel for use of facilities and materials at the Institute for Physiology in Bochum.

This work was supported by the Deutsche Forschungsgemeinschaft and the Fonds der Chemischen Industrie.

Received for publication 7 August 1997 and in revised form 3 August 1998.

References

Aarts, L.H.J., L.H. Schrama, W.J. Hage, J.L. Bos, W.H. Gispen, and P. Schotman. 1998. B-50/GAP-43-induced formation of filopodia depends on RhoGTPase. *Mol. Biol. Cell.* 9:1279–1292.

Adamson, P., C.J. Marshall, A. Hall, and P.A. Tilbrook. 1992. Post-translational modifications of p21rho proteins. *J. Biol. Chem.* 267:20033–20038.

Aigner, L., S. Arber, J.P. Kapfhammer, T. Laux, C. Schneider, F. Botteri, H.-R. Brenner, and P. Caroni. 1995. Overexpression of the neural growth-associated protein GAP-43 induces nerve sprouting in the adult nervous system of transgenic mice. *Cell.* 83:269–278.

Allen, L.H., and A. Aderem. 1995. A role for MARCKS, the α isozyme of protein kinase C and myosin I in zymosan phagozytosis by macrophages. *J. Exp. Med.* 182:829–840.

Babitch, J.A., T.B. Breithaupt, T.-C. Chiu, R. Garadi, and D.L. Helseth. 1976. Preparation of chick brain synaptosomes and synaptosomal membranes. *Biochim. Biophys. Acta.* 433:75–89.

Bordier, C. 1981. Phase separation of integral membrane proteins in Triton X-114 solution. *J. Biol. Chem.* 256:1604–1607.

Burwinkel, B., Y.S. Shin, H.D. Bakker, J. Deutsch, M.J. Lozano, I. Maire, and M.W. Kilimann. 1996. Mutation hotspots in the PHKA2 gene in X-linked liver glycogenosis due to phosphorylase kinase deficiency with atypical activity in blood cells (XLG2). *Hum. Mol. Genet.* 5:653–658.

Burwinkel, B., G. Miglierini, D.E. Jenne, D.J. Gilbert, N.G. Copeland, N.A. Jenkins, H.Z. Ring, U. Francke, and M.W. Kilimann. 1998. Structure of the human paralemmin gene (*PALM*), mapping to human chromosome 19p13.3 and mouse chromosome 10, and exclusion of coding mutations in *grizzled*, *mocha*, *jittery* and *hesitant* mice. *Genomics.* 49:462–466.

Cadwallader, K.A., H. Paterson, S.G. Macdonald, and J.F. Hancock. 1994. N-terminally myristoylated ras proteins require palmitoylation or a polybasic domain for plasma membrane localization. *Mol. Cell. Biol.* 14:4722–4730.

Caroni, P., L. Aigner, and C. Schneider. 1997. Intrinsic neuronal determinants locally regulate extrasynaptic and synaptic growth at the adult neuromuscular junction. *J. Cell Biol.* 136:679–692.

Chapman, E.R., R.P. Estep, and D.R. Storm. 1992. Palmitylation of neuromodulin (GAP-43) is not required for phosphorylation by protein kinase C. *J. Biol. Chem.* 267:25233–25238.

Clarke, S. 1992. Protein isoprenylation and methylation at carboxyl-terminal cysteine residues. *Annu. Rev. Biochem.* 61:355–386.

De Camilli, P., A. Thomas, R. Cofiell, F. Folli, B. Lichte, G. Piccolo, H.-M. Meinck, M. Austoni, G. Fassetta, G. Bottazzo, et al. 1993. The synaptic vesicle-associated protein amphiphysin is the 128-kD autoantigen of stiff-man syndrome with breast cancer. *J. Exp. Med.* 178:2219–2223.

Dekker, L.V., P.N.E. De Graan, A.B. Oestreicher, D.H.G. Versteeg, and W.H. Gispen. 1989. Inhibition of noradrenaline release by antibodies to B-50 (GAP-43). *Nature.* 342:74–76.

Dodt, G., N. Braverman, C. Wong, A. Moser, H.W. Moser, P. Watkins, D. Valle, and S.J. Gould. 1995. Mutations in the PTS1 receptor gene PXR1 define complementation group 2 of the peroxisome biogenesis disorders. *Nat. Genet.* 9:115–125.

Dropcho, E.J. 1996. Antiamphiphysin antibodies with small-cell lung carcinoma and paraneoplastic encephalomyelitis. *Ann. Neurol.* 39:659–667.

Evan, G.I., G.K. Lewis, G. Ramsay, and J.M. Bishop. 1985. Isolation of monoclonal antibodies specific for human c-myc proto-oncogene product. *Mol. Cell. Biol.* 5:3610–3616.

Feany, M.B., S. Lee, R.H. Edwards, and K.M. Buckley. 1992. The synaptic vesicle protein SV2 is a novel type of transmembrane transporter. *Cell.* 70:861–867.

Fischer, M., S. Kaech, D. Knutti, and A. Matus. 1998. Rapid actin-based plasticity in dendritic spines. *Neuron.* 20:847–854.

Gamby, C., M.C. Waage, R.G. Allen, and L. Baizer. 1996*a*. Growth-associated protein-43 (GAP-43) facilitates peptide hormone secretion in mouse anterior pituitary AtT-20 cells. *J. Biol. Chem.* 271:10023–10028.

Gamby, C., M.C. Waage, R.G. Allen, and L. Baizer. 1996*b*. Analysis of the role of calmodulin binding and sequestration in neuromodulin (GAP-43) function. *J. Biol. Chem.* 271:26698–26705.

Giannakouros, T., and A.I. Magee. 1992. Protein prenylation and associated modifications. *In* Lipid Modifications of Proteins. M.J. Schlesinger, editor. CRC Press, Boca Raton, FL. 135–162.

Gorgels, T.G.M.F., M. Van Lookeren Campagne, A.B. Oestreicher, A.A.M. Gribnau, and W.H. Gispen. 1989. B-50/GAP43 is localized at the cytoplasmic side of the plasma membrane in developing and adult rat pyramidal tract. *J. Neurosci.* 9:3861–3869.

Hagler, D.J., and Y. Goda. 1998. Synaptic adhesion: the building blocks of memory? *Neuron.* 20:1059–1062.

Hancock, J.F., K. Cadwallader, H. Paterson, and C.J. Marshall. 1991. A CAAX or a CAAL motif and a second signal are sufficient for plasma membrane targeting of ras proteins. *EMBO (Eur. Mol. Biol. Organ.) J.* 10:4033–4039.

Hartwig, J.H., M. Thelen, A. Rosen, P.A. Janmey, A.C. Nairn, and A. Aderem. 1992. MARCKS is an actin filament crosslinking protein regulated by protein kinase C and calcium-calmodulin. *Nature.* 356:618–622.

Hell, J.W., P.R. Maycox, H. Stadler, and R. Jahn. 1988. Uptake of GABA by rat brain synaptic vesicles isolated by a new procedure. *EMBO (Eur. Mol. Biol. Organ.) J.* 7:3023–3029.

Hens, J.J.H., F. Benfenati, H.B. Nielander, F. Valtorta, W.H. Gispen, and P.N.E. DeGraan. 1993. B-50/GAP-43 binds to actin filaments without affecting actin polymerization and filament organization. *J. Neurochem.* 61:1530–1533.

Hoesche, C., A. Sauerwald, R.W. Veh, B. Krippl, and M.W. Kilimann. 1993. The 5′-flanking region of the rat synapsin I gene directs neuron-specific and developmentally regulated reporter gene expression in transgenic mice. *J. Biol. Chem.* 268:26494–26502.

Hoesche, C., P. Bartsch, and M.W. Kilimann. 1995. The CRE consensus sequence in the synapsin I gene promoter region confers constitutive activation but no regulation by cAMP in neuroblastoma cells. *Biochim. Biophys. Acta.* 1261:249–256.

Holtmaat, A.J.G.D., P.A. Dijkhuizen, A.B. Oestreicher, H.J. Romijn, N.M.T. Van der Lugt, A. Berns, F.L. Margolis, W.H. Gispen, and J. Verhaagen. 1995. Direct expression of the growth-associated protein B-50/GAP-43 to olfactory neurons in transgenic mice results in changes in axon morphology and extraglomerular fiber growth. *J. Neurosci.* 15:7953–7965.

Johnston, G.C., J.A. Prendergast, and R.A. Singer. 1991. The *Saccharomyces cerevisiae* MYO2 gene encodes an essential myosin for vectorial transport of vesicles. *J. Cell Biol.* 113:539–551.

Karnik, S.S., K.D. Ridge, S. Bhattacharya, and H.G. Khorana. 1993. Palmitoylation of bovine opsin and its cysteine mutants in COS cells. *Proc. Natl. Acad. Sci. USA.* 90:40–44.

Karns, L.R., S.-C. Ng, J.A. Freeman, and M.C. Fishman. 1987. Cloning of complementary DNA for GAP-43, a neuronal growth-related protein. *Science.* 236:597–600.

Kennelly, P.J., and E.G. Krebs. 1991. Consensus sequences as substrate specificity determinants for protein kinases and protein phosphatases. *J. Biol. Chem.* 266:15555–15558.

Kloc, M., B. Reddy, S. Crawford, and L.D. Etkin. 1991. A novel 110-kDa maternal CAAX box-containing protein from Xenopus is palmitoylated and isoprenylated when expressed in baculovirus. *J. Biol. Chem.* 266:8206–8212.

Kloc, M., X.X. Li, and L.D. Etkin. 1993. Two upstream cysteines and the CAAX motif but not the polybasic domain are required for membrane association of Xlcaax in Xenopus oocytes. *Biochemistry.* 32:8207–8212.

Lichte, B., R.W. Veh, H.E. Meyer, and M.W. Kilimann. 1992. Amphiphysin, a novel protein associated with synaptic vesicles. *EMBO (Eur. Mol. Biol. Organ.) J.* 11:2521–2530.

Magee, T., and C. Newman. 1992. The role of lipid anchors for small G proteins in membrane trafficking. *Trends Cell Biol.* 2:318–323.

McNew, J.A., M. Sögaard, N.M. Lampen, S. Machida, R.R. Ye, L. Lacomis, P. Tempst, J.E. Rothman, and T.H. Söllner. 1997. Ykt6p, a prenylated SNARE essential for endoplasmic reticulum-Golgi transport. *J. Biol. Chem.* 272: 17776–17783.

Mercer, J.A., P.K. Seperack, M.C. Strobel, N.G. Copeland, and N.A. Jenkins. 1991. Novel myosin heavy chain encoded by murine dilute coat colour locus. *Nature.* 349:709–713.

Ouimet, C.C., J.K.T. Wang, S.I. Walaas, K.A. Albert, and P. Greengard. 1990. Localization of the MARCKS (87 kDa) protein, a major specific substrate for protein kinase C, in rat brain. *J. Neurosci.* 10:1683–1698.

Pastural, E., F.J. Barrat, R. Dufourcq-Lagelouse, S. Certain, O. Sanal, N. Jabado, R. Seger, C. Griscelli, A. Fischer, and G. de Saint Basile. 1997. Griscelli disease maps to chromosome 15q21 and is associated with mutations in the myosin-Va gene. *Nat. Genet.* 16:289–292.

Prekeris, R., and D.M. Terrian. 1997. Brain myosin V is a synaptic vesicle-associated motor protein: Evidence for a Ca^{2+}-dependent interaction with the synaptobrevin–synaptophysin complex. *J. Cell Biol.* 137:1589–1601.

Pryde, J.G. 1986. Triton X-114: A detergent that has come in from the cold. *Trends Biochem. Sci.* 11:160–163.

Rechsteiner, M., and S.W. Rogers. 1996. PEST sequences and regulation by proteolysis. *Trends Biochem. Sci.* 21:267–271.

Ryan, T.A. 1998. Probing a complex question: when are SNARE proteins ensnared? *Nat. Neurosci.* 1:175–177.

Sanders, G., B. Lichte, H.E. Meyer, and M.W. Kilimann. 1992. cDNA encoding the chicken ortholog of the mouse dilute gene product. *FEBS (Fed. Eur. Biochem. Soc.) Lett.* 311:295–298.

Shupliakov, O., P. Löw, D. Grabs, H. Gad, H. Chen, C. David, K. Takei, P. De Camilli, and L. Brodin. 1997. Synaptic vesicle endocytosis impaired by disruption of dynamin-SH3 domain interactions. *Science.* 276:259–263.

Songyang, Z., K.L. Carraway III, M.J. Eck, S.C. Harrison, R.A. Feldman, M. Mohammadi, J. Schlessinger, S.R. Hubbard, D.P. Smith, C. Eng, et al. 1995. Catalytic specificity of protein tyrosine kinases is critical for selective signalling. *Nature*. 373:536–539.

Songyang, Z., K.P. Lu, Y.T. Kwon, L.-H. Tsai, O. Filhol, C. Cochet, D.A. Brickey, T.R. Soderling, C. Bartleson, et al. 1996. A structural basis for substrate specificities of protein Ser/Thr kinases: primary sequence preference of casein kinases I and II, NIMA, phosphorylase kinase, calmodulin-dependent kinase II, CDK5, and Erk1. *Mol. Cell. Biol.* 16:6486–6493.

Strittmatter, S.M., S.C. Cannon, E.M. Ross, T. Higashijima, and M.C. Fishman. 1993. GAP-43 augments G protein-coupled receptor transduction in Xenopus laevis oocytes. *Proc. Natl. Acad. Sci. USA*. 90:5327–5331.

Strittmatter, S.M., D. Valenzuela, and M.C. Fishman. 1994. An amino-terminal domain of the growth-associated protein GAP-43 mediates its effects on filopodial formation and cell spreading. *J. Cell Sci.* 107:195–204.

Strittmatter, S.M., C. Fankhauser, P.L. Huang, H. Mashimoto, and M.C. Fishman. 1995. Neuronal pathfinding is abnormal in mice lacking the neuronal growth cone protein GAP-43. *Cell.* 80:445–452.

Stumpo, D.J., C.B. Bock, J.S. Tuttle, and P.J. Blackshear. 1995. MARCKS deficiency in mice leads to abnormal brain development and perinatal death. *Proc. Natl. Acad. Sci. USA*. 92:944–948.

Van Lookeren Campagne, M., A.B. Oestreicher, P.M.P. Van Bergen en Henegouwen, and W.H. Gispen. 1990. Ultrastructural double localization of B-50/GAP43 and synaptophysin (p38) in the neonatal and adult rat hippocampus. *J. Neurocytol.* 19:948–961.

Verhaagen, J., W.T.J.M.C. Hermens, A.B. Oestreicher, W.H. Gispen, S.D. Rabkin, D.W. Pfaff, and M.G. Kaplitt. 1994. Expression of the growth-associated protein B-50/GAP43 via a defective herpes-simplex virus vector results in profound morphological changes in non-neuronal cells. *Mol. Brain Res.* 26:26–36.

Wang, F.-S., J.S. Wolenski, R.E. Cheney, M.S. Mooseker, and D.G. Jay. 1996. Function of myosin-V in filopodial extension of neuronal growth cones. *Science.* 273:660–663.

Wang, X., and M.W. Kilimann. 1997. Identification of two new μ-adaptin-related proteins, μ-ARP1 and μ-ARP2. *FEBS (Fed. Eur. Biochem. Soc.) Lett.* 402:57–61.

Weber, T., B.V. Zemelman, J.A. McNew, B. Westermann, M. Gmachl, F. Parlati, T.H. Söllner, and J.E. Rothman. 1998. SNAREpins: minimal machinery for membrane fusion. *Cell.* 92:759–772.

Widmer, F., and P. Caroni. 1993. Phosphorylation-site mutagenesis of the growth-associated protein GAP-43 modulates its effects on cell spreading and morphology. *J. Cell Biol.* 120:503–512.

Wiederkehr, A., J. Staple, and P. Caroni. 1997. The motility-associated proteins GAP-43, MARCKS, and CAP-23 share unique targeting and surface activity-inducing properties. *Exp. Cell Res.* 236:103–116.

Wüllrich, A., C. Hamacher, A. Schneider, and M.W. Kilimann. 1993. The multiphosphorylation domain of the phosphorylase kinase αM and αL subunits is a hotspot of differential mRNA processing and of molecular evolution. *J. Biol. Chem.* 268:23208–23214.

Yankner, B.A., L.I. Benowitz, L. Villa-Komaroff, and R.L. Neve. 1990. Transfection of PC12 cells with the human GAP-43 gene: effects on neurite outgrowth and regeneration. *Mol. Brain Res.* 7:39–44.

Zuber, M.X., D.W. Goodman, L.R. Karns, and M.C. Fishman. 1989. The neural growth-associated protein GAP-43 induces filopodia in non-neuronal cells. *Science.* 244:1193–1195.